Seven years of IASI ozone retrievals from FORLI: validation with independent total column and vertical profile measurements

Anne Boynard[1], Daniel Hurtmans[2], Mariliza E. Koukouli[3], Florence Goutail[1], Jérôme Bureau[1], Sarah Safieddine[4], Christophe Lerot[5], Juliette Hadji-Lazaro[1], Jean-Pierre Pommereau[1], Andrea Pazmino[1], Irene Zyrichidou[3], Dimitris Balis[3], Alain Barbe[6], Semen N. Mikhailenko[7,8], Diego Loyola[9], Pieter Valks[9], Michel Van Roozendael[5], Pierre-François Coheur[2], and Cathy Clerbaux[1,2]

[1]LATMOS/IPSL, UPMC Univ. Paris 06 Sorbonne Universités, UVSQ, CNRS, Paris, France
[2]Spectroscopie de l'Atmosphère, Chimie Quantique et Photophysique, Université Libre de Bruxelles (U.L.B.), Brussels, Belgium
[3]Laboratory of Atmospheric Physics, Aristotle University of Thessaloniki, Thessaloniki, Greece
[4]Department of Civil and Environmental Engineering, Massachusetts Institute of Technology, Cambridge, MA, USA
[5]Belgian Institute for Space Aeronomy, Brussels, Belgium
[6]Université de Reims-Champagne-Ardenne, Groupe de Spectrométrie Moléculaire et Atmosphérique, 51062 Reims, France
[7]V.E. Zuev Institute of Atmospheric Optics, SB, Russian Academy of Science, 1, Akademician Zuev Square, 634021 Tomsk, Russia
[8]Climate and Environmental Physics Laboratory, Ural Federal University, 19, Mira Avenue, 620002 Yekaterinburg, Russia
[9]Institut für Methodik der Fernerkundung (IMF), Deutsches Zentrum für Luft- und Raumfahrt (DLR), Oberpfaffenhofen, Germany

Correspondence to: Anne Boynard (anne.boynard@latmos.ipsl.fr)

Abstract. This paper presents an extensive inter-comparison and validation for the ozone (O_3) product measured by the two Infrared Atmospheric Sounding Interferometers (IASI) launched onboard the Metop-A and Metop-B satellites in 2006 and in 2012, respectively. IASI O_3 total columns and vertical profiles obtained from Fast Optimal Retrievals on Layers for IASI (FORLI-O3) v20140922 software (running up until recently) are validated against independent observations during the period 2008-2014 on a global scale. On average for the period 2013-2014, IASI-A and IASI-B TOCs retrieved using FORLI are consistent, with IASI-B providing slightly lower values with a global difference of only 0.2±0.8%. The comparison between IASI-A and IASI-B O_3 vertical profiles shows differences within ±2% over the entire altitude range. Global validation results for seven years of IASI TOCs from FORLI against GOME-2/Metop-A, Dobson and Brewer data show that, on average, IASI overestimates the UV data by 5-6% with the largest differences found in the Southern high latitudes. The comparison with UV-vis SAOZ measurements shows a mean bias between IASI and SAOZ TOCs of 2-4% in the mid-latitudes and tropics, and 7% at the polar circle. Part of the discrepancies found at high latitudes can be attributed to the limited information content in the observations, due to low brightness temperatures. The comparison with ozonesonde vertical profiles (limited to 30 km) shows that on average IASI with FORLI processing underestimates O_3 by ~5-15% in the troposphere while it overestimates O_3 by ~10-40% in the stratosphere depending on the latitude. In the Northern middle latitudes, the bias varies within ±20% for the entire altitude range. The largest relative differences are found in the tropical tropopause region; this can be explained by the low O_3 amounts leading to large relative errors. In this study, we also evaluate an updated version of FORLI-O3 retrieval software (v20151001), using look-up tables recalculated to cover a larger

spectral range using the latest HITRAN spectroscopic database (HITRAN 2012), and implementing numerical corrections. The assessement of the new O_3 product with the same set of observations as that used for the validation exercise shows a correction of ~4% for the TOC positive bias when compared to the UV ground-based and satellite observations, bringing the overall global comparison to ~1-2% on average. This improvement is mainly associated with a decrease in the retrieved O_3

5   concentration in the stratosphere (above 30 hPa/25 km) as shown by the comparison with ozonesonde data.

1 Introduction

Despite its small amount, ozone (O_3) plays very significant roles in the atmosphere. In the stratosphere, O_3 protects the biosphere and humans from harmful ultraviolet (UV) radiation. In contrast, O_3 in the troposphere is considered as one of the main air pollutants impacting both human health (Brunekreef and Holgate, 2002; Lim et al., 2012) and ecosystems (Fowler

10   et al., 2009). Tropospheric O_3 originates either from complex photochemical reactions involving nitrogen oxides (NO_x), carbon monoxide (CO) and hydrocarbons (e.g. Chameides and Walker, 1973; Crutzen, 1973) or from the stratosphere by downward transport to the troposphere especially at mid- and high latitudes (e.g. Holton et al., 1995). Tropospheric O_3 is the third most important anthropogenic greenhouse gas after carbon dioxide and methane (IPCC, 2013) and is referred to as a short-lived climate forcing constituent (Shindell et al., 2012). In particular, upper tropospheric O_3 affects global outgoing

15   long wave radiation (Worden et al., 2008) and its changes have a significant impact on the surface temperature (IPCC, 2013). Enhanced upper tropospheric O_3 can impact air quality when transported to the boundary layer (Fiore et al., 2002). The lifetime of tropospheric O_3 varies with altitude and ranges from 1-2 days in the boundary layer where dry deposition is the major sink to several weeks in the free troposphere (e.g. Stevenson et al., 2006), which is sufficiently long for O_3 to be transported intercontinentally (Monks et al., 2015). Thus O_3 can influence air quality from urban scale to hemispheric scale

20   (e.g. HTAP, 2010) and there is an obvious need to treat O_3 across this range of scales. To this end, new observational opportunities are offered by both satellites and small sensors that bridge the scales (Monks et al., 2015).

Space observation in the nadir geometry is the most efficient way to obtain global information on horizontal distribution of O_3, along with coarse information on the vertical. However, retrievals of tropospheric O_3 remain challenging since most of the O_3 is contained in the stratospheric O_3 layer, and the satellite signal integrates both contributions. The first distributions

25   of tropospheric O_3 were derived from UV-visible measurements by subtracting an estimate of the stratospheric component from the measured total column (e.g. Fishman and Larsen, 1987; Fishman et al., 1990). More recently several studies have developed alternative approaches to tropospheric O_3 retrieval from nadir-viewing satellite UV spectrometers to have sensitivity to tropospheric O_3 (e.g. Miles et al., 2015; Valks et al., 2014).

However, the recently developed thermal infrared (TIR) nadir-viewing spectrometers offer more sensitivity in the

30   troposphere, as demonstrated by the Tropospheric Emission Spectrometer (TES) on board EOS-AURA (e.g. Nassar et al., 2008; Worden et al., 2007) and the Infrared Atmospheric Sounding Instrument (IASI) on board MetOp-A and B (e.g. Boynard et al., 2009; Dufour et al., 2012). TES and IASI have provided measurements of tropospheric O_3 for a large range

of applications: atmospheric composition (Boynard et al., 2009; Wespes et al., 2012, 2015), transport (Jones et al., 2008), climate (Doniki et al., 2015; Worden et al., 2008) and air quality (Dufour et al., 2010, 2015; Eremenko et al., 2008; Safieddine et al., 2013, 2014; Verstraeten et al., 2015). Recently, the ability of IASI to detect boundary layer pollution in case of large negative thermal contrast combined with high levels of pollution provided a first step towards the use of TIR

5 sounders to contribute to air quality monitoring, evaluation and management (Boynard et al., 2014).

Initial validation of IASI total and tropospheric O_3 was carried out by Boynard et al. (2009). The paper compares a year of IASI-A measurements to both UV satellite and ground-based observations along with ozonesonde data. More recently IASI O_3 has been validated against independent observations in a series of papers (Antón et al., 2011; Dufour et al., 2012; Gazeaux et al., 2013; Pommier et al., 2012; Oetjen et al., 2014; Safieddine et al., 2015; Scannell et al., 2012; Toihir et al.,

10 2015). These papers report that the comparisons between IASI and UV instruments show a bias for the total column ranging from ~3% (Brewer/Dobson) to ~6% (GOME-2A) on the global scale. For the vertical profile, the bias is generally lower than 10%, except in the 10-25 km altitude range where a positive bias of 10-15% is reported (Dufour et al., 2012; Gazeaux et al., 2013). However, these different studies focused on a particular region and/or a relatively short period of time.

The purpose of the present paper is to provide an update on the O_3 retrievals using the Fast Optimal Retrievals on Layers for

15 IASI (FORLI-O3) software (Hurtmans et al., 2012) that allows to systematically retrieve global distributions of O_3 vertical profiles in a near-real time mode. The main aim of this work is (1) to extend the IASI-A O_3 validation to the 2008-2014 period and with a range of different instruments such as satellite sensors, Brewer/Dobson spectrophotometers, SAOZ instruments and ozonesondes, and (2) to quantify the consistency between the O_3 retrieved by the second IASI instrument (IASI-B) with that of IASI-A. The next section provides a description of the IASI O_3 measurements including the IASI

20 instrument and the O_3 profile retrieval processing. Section 3 presents an inter-comparison between O_3 derived from IASI-A and IASI-B. In Section 4 and 5 the results of the validation of total O_3 columns (TOCs) and vertical profiles are presented, respectively. Section 6 provides preliminary results on an updated version of the retrieval algorithm. Conclusions are given in Section 7.

2 IASI ozone retrievals

25 ### 2.1 The IASI instrument

IASI was designed for operational meteorology and for monitoring atmospheric chemistry and climate. It is a TIR Fourier transform spectrometer (Clerbaux et al., 2009, 2015) on-board the MetOp-A and B satellites, which were launched in October 2006 and September 2012, respectively. The launch of the third and last satellite (MetOp-C) is scheduled for 2018. The role of MetOp-C is to ensure the continuity of observations from a polar orbit started at the beginning of the Metop

30 mission. The IASI instruments will provide homogeneous long term data sets of 15 years related to atmospheric composition.

Atmospheric
Measurement
Techniques
Discussions

Both IASI-A and -B instruments have been operationally sounding the atmosphere since October 2007 and March 2013, respectively. The Metop-A and B satellites are on a polar, sun-synchronous orbit (about 817 km altitude) with Equator crossing times of 9:30 (21:30) local mean solar time for the descending (ascending) part of the orbit. IASI is nadir viewing and mesures the radiation emitted from the Earth's surface and absorbed and emitted by the atmosphere in the TIR spectral

5   range, between 645 and 2760 cm^{-1} with an apodized spectral resolution of 0.5 cm^{-1} and radiometric noise of 0.2 K (for a reference temperature of 280 K) in the O_3 spectral absorption region (near 9.6 μm). Because of the nadir geometry complemented by off-nadir measurements up to 48.3° on both sides of the satellite track (swath of about 2200 km), each IASI instrument covers the globe twice a day, providing more than 1.3 million spectra each day. At nadir, each IASI instantaneous field of view is composed of four individual ground pixels of 12 km diameter each.

10   The two MetOp satellites are on the same orbit with a 180° shift, therefore there are numerous common observations between two consecutive tracks. However there is a ~50 min temporal shift between both instruments (one satellite might be before or after the other), thus the observations are never simultaneous. In addition, the geometry of the observations is different and generally off-nadir with opposite angles, so the location of the observation between the two instruments varies and thus the pixels are not geographically co-localized.

15   **2.2 Ozone retrievals with FORLI**

Retrievals of O_3 global distributions have been systematically performed in a near-real time mode using the FORLI-O3 v20140922 software (Hurtmans et al., 2012), which was until a few weeks ago the reference FORLI version. In this study we used the IASI-A and IASI-B O_3 data retrieved from January 2008 and from March 2013, respectively, until December 2014. FORLI-O3 is based on the optimal estimation method (OEM) (Rodgers, 2000) and relies on tabulated absorption cross-

20   sections at various pressures and temperatures to speed up the radiative transfer calculation. The OEM uses *a priori* information to constrain ill-posed problems such as O_3 concentration retrievals from nadir-viewing spaceborne sounders. The OEM also provides an error budget associated with the retrievals and diagnostic variables allowing accurate comparisons with other data. In particular, the averaging kernel matrix characterizing the sensitivity of the retrieved state to the true state is provided for each retrieval. The position of its peak gives the altitude of maximum sensitivity, while its full width at half

25   maximum is an estimation of the vertical resolution of the retrieved state (Rodgers, 2000). The trace of this matrix, called Degrees Of Freedom For Signal (DOFS), represents the number of independent pieces of information contained in the measurements, which gives an estimation of the vertical sensitivity of the retrievals.

The O_3 retrieval spectral range is 1025-1075 cm^{-1}, which is dominated by O_3 lines with only few water vapor lines and a weak absorption contribution of methanol (Hurtmans et al., 2012). The *a priori* covariance matrix $\mathbf{S}_a$ is constructed from the

30   McPeters/Labow/Logan climatology of O_3 profiles, which combines long-term satellite limb observations and measurements from O_3 sondes (McPeters et al., 2007). The *a priori* profile $\boldsymbol{x}_a$ is the mean of the ensemble. The O_3 product from FORLI is a vertical profile retrieved on 40 layers between surface and 40 km, with an extra layer from 40 km to the top of the atmosphere. Due to the enormous amount of data, retrievals are only performed for clear or almost-clear scenes with a

Atmospheric
Measurement
Techniques
Discussions

fractional cloud cover below 13%, identified using the cloud information from the Eumetsat operational processing (August et al., 2012). A second filter is applied to keep only the more reliable data, by removing those corresponding to poor spectral fits (root mean square (RMS) of the spectral fit residual higher than 3.5×10^{-8} W cm^{-2} sr cm^{-1}). For a full description of the FORLI-O3 software and the OEM algorithm the reader is referred to Hurtmans et al. (2012).

5   Figure 1 provides an example of O_3 monitoring with IASI-A. It illustrates the evolution of O_3 hole over 2008-2015, with the distribution of TOCs obtained above Antarctica averaged over one month between 12 September and 12 October for each year. This figure highlights the good capability of IASI to capture the spatial and temporal variability of TOCs in the Antarctic region. It is worth noting that the O_3 hole size is larger in 2015 than in the previous years (integrated over the same time period) as shown by Fig. 1. According to the World Meteorological Organization (WMO), this larger O_3 hole in 2015 is

10   due to unusually cold temperature and weak dynamics in the Antarctic stratosphere.

Previous studies have shown that the sensitivity of IASI to tropospheric O_3 is generally maximum between 6 and 8 km, with some seasonal variability (e.g. Clerbaux et al., 2015). However in case of significant thermal contrast (i.e. the difference of temperature between the ground and the atmospheric layer just above it), the sensitivity of IASI increases near the ground. Typical averaging kernel functions associated with high (26 K), medium (11 K) and low (1 K) thermal contrast are

15   illustrated in Fig. 2. The averaging kernels are given for four different atmospheric layers as defined in Wespes et al. (2015): surface-300 hPa, 300-150 hPa, 150-25 hPa and 25-3 hPa, characterizing the troposphere (TROPO), the upper troposphere and the lower stratosphere (UTLS), the middle stratosphere (MS) and the upper stratosphere (US), respectively. As can be seen from these plots, in case of low thermal contrast, two partial columns (300-150 hPa, 150-25 hPa) can be retrieved independently, and the sensitivity of IASI in the troposphere is maximum around 8 km. In case of medium thermal contrast,

20   the information can be presented by three prominent averaging kernels, corresponding to the surface-300 hPa, 300-150 hPa, 150-25 hPa partial columns. In this case the IASI sensitivity to the troposphere peaks around 6 km. Finally, in case of high thermal contrast, three partial columns can also be retrieved, but with a sensitivity to the troposphere increasing down to the lower troposphere (around 3-4 km).

The uncertainty on the O_3 profile retrievals depends on the latitude and the season, reflecting, amongst other, the influence of

25   signal intensity and thermal contrast (Wespes et al., 2015). It generally varies between 10 and 30% in the troposphere and in the UTLS, and 5% in the stratosphere. However larger relative errors are found in the tropics, which are linked with the low O_3 amounts (Wespes et al., 2015).

3 Intercomparison between IASI-A and IASI-B ozone content

Several inter-comparison exercises between IASI-A and IASI-B radiance spectra have been performed in the framework of

30   the Global Space Based Inter-Calibration System (GSICS; http://gsics.wmo.int/). An excellent consistency between both sensors has been demonstrated, with radiometric biases lower or equal to 0.1 K and spectral biases lower than 1 ppm, which

Atmospheric
Measurement
Techniques
Discussions

is compliant with the specification of 0.5 K and 2 ppm, respectively (see IASI quarterly performance reports here: https://iasi.cnes.fr/fr/IASI/Fr/lien1_car_instr.htm).

The comparison between IASI-A and IASI-B O_3 products retrieved with FORLI is not straightforward since the pixels are not co-localized in time and space. In addition each IASI O_3 measurement is associated with a cloud flag (see Section 2), so one observation seen at a certain location with IASI-A might be contaminated by clouds and filtered out in the retrievals processing, while it might not be the case with IASI-B. An easy way out to compare IASI-A and IASI-B O_3 products is to average observations on a daily basis over a constant grid; this is what is discussed next, using a 1°x1° grid.

A statistical analysis of IASI-A and IASI-B TOCs was performed with respect to time and latitude for the year 2014. Figure 3 illustrates the monthly mean relative differences of TOCs for the year 2014 as a function of month and latitude for day time measurements (left panel) and nighttime measurements (right panel). IASI pixels are considered day time and nighttime data if the solar zenith angle (SZA) is <90° and >=90°, respectively. An excellent agreement between both IASI-A and IASI-B TOCs is observed, with differences generally within 1% for all latitudes, which could be due to both the temporal gap and the different observation geometry leading to different sampling of IASI-A and IASI-B. The larger differences found locally can be attributed to the low numbers of IASI pixels within a 1°x1° grid cell. Another possible reason for the differences, especially in polar regions, is the overlap by consecutive orbits with different time and thus, different meteorological conditions, and also to different azimuth angles. On average for the period 2013-2014, IASI-A and IASI-B TOCs retrieved using FORLI are consistent, with IASI-B providing slightly lower values with a global difference of only 0.2±0.8%.

We investigated in more detail the differences between IASI-A and IASI-B O_3 by performing a comparison of the FORLI O_3 vertical profiles. Figure 4 shows the monthly mean relative differences of O_3 vertical profiles for the year 2014 as a function of month and altitude for different latitude bands. Overall the differences between IASI-A and IASI-B O_3 concentrations are within ±2% for the entire altitude range. IASI-A tends to measure less O_3 in the troposphere and the upper stratosphere and more O_3 in the middle stratosphere compared to IASI-B. Locally, larger differences are also found, especially in the Antarctic region (values < -10% in the 10-15 km altitude range for the January-July period) and in the Northern mid-latitudes (differences up to -6% in the spring season). The lower differences are found above 20 km, where most of O_3 is located (differences < 0.5%). The main differences are in the troposphere and close to the surface: on average IASI-A measures 2.0±0.2% less tropospheric O_3 than IASI-B. As shown in Fig. 5 the standard deviation of the relative differences between IASI-A and IASI-B O_3 vertical profiles ranges between 5% and 20% for the entire altitude range and is larger in the tropopause region, characterized by low O_3 concentrations, large natural variability and a strong dependency on the tropopause altitude. The variability is much larger in the Antarctic region (>=20%) for the January-August period, which may be attributed to the overlap by consecutive orbits with different time and thus, different air masses.

This section shows an excellent agreement between IASI-A and IASI-B O_3 total columns and vertical profiles: differences within 1% and 2% are found for the TOCs and the vertical profiles, respectively.

Atmospheric
Measurement
Techniques
Discussions

4 Validation of total ozone column

4.1 Comparison with GOME-2 retrievals

The Global Ozone Monitoring Experiment-2 (GOME-2) instrument, also on board the MetOp-A and B platforms, is a UV-VIS-NIR nadir viewing spectrometer covering the spectral range from 240 to 790 nm with a spectral sampling of 0.11-0.22

5   nm and a spectral resolution of 0.24-0.53 nm (Munro et al., 2015). The maximum swath is about 1920 km providing almost global coverage of the sunlit part of the atmosphere within one day. The reader is kindly referred to Munro et al. (2015) for a full description of the instrument design, calibration and L1 processing, and to Hassinen et al. (2015) for a description of the full suite of GOME-2 L2 operational products. In this study, two different TOC products from GOME-2/MetOp-A (GOME-2A) were used for the validation of IASI TOCs from FORLI: (1) GOME-2 TOC data that has been generated as part of the

10   Eumetsat Ozone Monitoring and Atmospheric Composition Satellite Application Facility (O3M SAF) with the GOME Data Processor (GDP) operational algorithm, which is an iterative DOAS-AMF fitting algorithm and uses the ozone absorption features in Huggins band between 325 and 335 nm (Loyola et al., 2011; Hao et al., 2014), and (2) GOME-2 TOC data generated as part of the ESA Ozone Climate Change Initiative (O3-CCI) with the GOME-type Direct Fitting algorithm (GODFIT) (Van Roozendael et al., 2012; Lerot et al., 2014) and publicly available on http://www.esa-ozone-cci.org. The

15   GOME-2 O3M SAF and CCI TOC products have been validated using ground-based measurements (e.g Hao et al., 2014; Koukouli et al., 2012, 2015; Loyola et al., 2011), which has shown an overall agreement within 1% in most situations. Note that in this section (and in Section 6) only the results related to the IASI and GOME-2A TOC data generated within the Eumetsat O3M SAF are presented.

For the validation of IASI TOC retrievals from FORLI, IASI and GOME-2A TOC distributions were averaged over a

20   constant 1°x1° grid and compared over the period 2008-2014. As the UV-vis instrument provides day time observations, only the IASI day time data (SZA < 90°) are used in this comparison. Figure 6 shows the global distributions of TOCs obtained from the IASI-A and GOME-2A O3M SAF retrievals along with the associated relative differences for different seasons of the period 2008-2014. Although, when compared to GOME-2A, IASI-A overestimates O_3, similar spatial and seasonal patterns are observed by both instruments. The spatial distribution of total O_3 varies strongly with latitude, the

25   largest values occurring at mid- and high latitudes during all seasons. This is due to the production rates of O_3 from solar UV radiation that are generally highest in the tropics and the large-scale air circulation in the stratosphere that transports O_3 from the tropics toward the poles (Dessler, 2000). This results in O_3 accumulation at mid- and high latitudes, increasing the O_3 layer thickness and thus total O_3. In contrast, the lowest values of total O_3 are located in the tropics for all seasons (except for the O_3 hole season in Sep-Oct-Nov) because the O_3 layer is smaller there (Dessler, 2000). Little seasonal change in total O_3

30   is found in the tropics compared to the polar regions. This is due to the smaller seasonal changes in both sunlight and O_3 transport in the tropics than in polar regions. The annual O_3 depletion over the Antarctic in the austral spring season (September-October-November) is well observed by both instruments. It is worth mentioning that in contrast to UV-vis instruments (e.g. GOME-2 and OMI), IASI can measure the ozone distribution over the whole South Pole region during

austral winter. The largest differences between the two instruments are observed over Antarctica during the austral summer and fall seasons and will be discussed hereafter.

Figure 7 shows the temporal evolution of the relative difference between IASI-A in blue and IASI-B in red against GOME-2A O3M SAF gridded TOCs along with the standard deviation for different latitudinal bands. The three main features that arise from this figure are (1) the excellent agreement between the IASI-A and the IASI-B comparisons, (2) the systematic overestimation of IASI with FORLI processing and (3) the pronounced seasonality in the difference between IASI and GOME-2A TOCs, the lowest differences being found in summer and the largest differences in winter. A possible reason for this seasonality can be attributed to the lower sensitivity of IASI in winter generally characterized to lower brightness temperature. The seasonal variation is less pronounced in the middle latitudes and the tropics than in the polar regions, which is due to the more pronounced seasonal cycle of photochemical activity and the larger seasonal change in transport at high latitudes. The lowest differences are found in the middle latitudes (2-4%) and the tropics (~4-6%) while the highest differences are found at high latitudes, especially over Antarctica (up to 30% during the austral summer season). Possible reasons for these differences are i) the ~4% disagreement between the ozone absorption coefficients in the IR and UV spectral regions (Picquet-Varrault et al., 2005; Gratien et al., 2010); ii) the limited information content in the IASI observations at high latitudes due to low brightness temperatures; iii) the temperature profiles used in FORLI that are less reliable in Antarctica (August et al., 2012); and iv) the errors associated to TOC retrievals in the UV-vis spectral range increasing at high solar zenith angles, mostly because of the larger sensitivity of the retrieval to the *a priori* O_3 profile shape (Lerot et al., 2014). It is worth noting that in the tropics there is a small drift visible in the last two years (2013-2014), which is not apparent in the comparisons between IASI and ground-based TOCs (see Figures 10 and 11). This may be related to the instrumental degradation of GOME-2A in recent years (Munro et al., 2015).

Table 1 gives some statistics related to the differences between IASI-A with FORLI processing and GOME-2A O3M SAF TOCs separately for each season, at global scale and for six different latitude zones. Globally, IASI-A and GOME-2A are in good agreement, with coefficients of correlation ranging from 0.93 to 0.98 and a positive bias from IASI-A of 5.5 to 7.1% depending on the season. On average, over the period 2008-2014, the bias value is around 6.2±7.5%, which is of the same order as the bias reported in Antón et al. (2011). The detailed analysis undertaken for different latitude bands shows that the highest correlation coefficients are found in the mid-latitude regions, with values higher than 0.93. Poor correlation is found between IASI-A and GOME-2A in the high latitudes of the Southern hemisphere (SH) during austral summer and fall. Further investigation for Antarctica needs to be performed to understand the reasons for these discrepancies. However during the O_3 hole season, high correlation of 0.96 is found in the Southern polar region, with IASI-A TOCs being positively biased (~11.6%). This suggests that IASI underestimates the extent of O_3 depletion with respect to GOME-2A.

4.2 Comparison with gound-based spectrophotometer data

Complementary to space observations, total O_3 is routinely measured at ground stations by the Brewer and Dobson instruments (Fioletov et al., 2008). These ground-based observations considered as the "ground-truth" standard for TOC

measurements are publicly available at the World Ozone and Ultraviolet Radiation Data Centre (WOUDC, http://woudc.org). The total O_3 measurement of the Brewer and Dobson instruments relies on the method of differential absorption in the Huggins band where O_3 exhibits strong absorption features in the UV part of the solar spectrum. Compared to the Dobson instrument, the Brewer spectrophotometer has an improved optical design and is fully automated. The TOC

5   abundance is determined from a combination of four wavelengths between 306 nm and 320 nm with a resolution of 0.6 nm overcoming the spectral interference of sulphur dioxyde with O_3 (Kerr et al., 1984; Kerr, 2002). The Dobson and Brewer stations considered in this paper and the criteria used for the selection of the stations have been extensively used in a series of validation papers of satellite total O_3 measurements (e.g. Balis et al., 2007a, 2007b; Koukouli et al., 2012, 2015; Weber et al., 2005).

10   For the comparisons with IASI TOCs from FORLI, only direct sun observations are used as those are the most reliable for both the Dobson and the Brewer spectrophotometers, the latter offering an accuracy of about 1% at moderate solar zenith angles. All data available for the period 2008-2014 have been extracted. The data format currently used consists of daily total O_3 values expressed in Dobson units (DU). We set the coincidence criteria to a 50 km search radius between the satellite centre of pixel and the geocolocation of the ground-based station as well as to the same day of observations. All

15   IASI TOCs meeting the above criteria were then averaged. In total 47 Brewer and 53 Dobson stations were considered for the comparison. The locations of the stations are represented in Fig. 8 and listed in Table 2. As illustrated in Fig. 8, a wide geographical region is covered by the network of ground-based instruments, with fair sampling of all latitudes. More specifically, apart from three Antarctic stations, the Brewer network mostly represents the Northern hemisphere (NH), whereas the Dobson network is more balanced in terms of latitude coverage. Also note that the most represented latitudinal

20   region is that of the Northern middle latitudes for both types of instrument. Both IASI-A and IASI-B were compared to the ground-based observations. For the comparison with IASI-B, the ground-based dataset was reduced to contain only the common co-locations between the two space-borne instruments and the respective ground-based one during the period March 2013 – December 2014.

Figure 9 shows the relative differences between IASI-A in blue and IASI-B in red and the ground-based TOCs averaged

25   over 10° latitude bands for the period 2008-2014 and 2013-2014, respectively. Very similar features between the IASI-A and IASI-B comparisons can be seen, with the Antarctic being largely over-estimated (up to 20% and beyond) and the Northern middle latitudes driving the mean comparisons around the 4% to 6% level. Larger differences are also seen in the Southern mid-latitudes (up to 8%) and in the Northern high latitudes (up to 9%). The larger differences found at high latitudes are consistent with the results found for the IASI/GOME-2A comparison (see Fig. 6 and 7) and part of them is attributed to the

30   limited information content in the observations, due to low brightness temperatures. Figure 10 shows the time series of monthly mean differences between IASI-A and IASI-B against Dobson and Brewer TOCs for the period 2008-2014 for the NH. IASI with FORLI processing overestimates total O_3 abundance compared to the Dobson and Brewer instruments. The mean difference between IASI and Dobson measurement is ~5±1% for the NH, whereas it is slightly larger (~6±1%) for the SH. A similar picture is revealed by the Brewer network comparisons, with a mean difference between IASI and Brewer

TOCs of ~4±1%. Similar results are found for the comparison between IASI and Dobson in the SH (not shown here). As for the IASI/GOME-2A TOC comparison, an obvious seasonal variability in the difference between IASI and ground-based TOCs is visible with the lowest difference in summer and the largest differences in winter.

4.3 Comparison with ground-based SAOZ data

The SAOZ (Système d'Analyse par Observation Zénithale) is a zenith sky UV-vis spectrometer developed by Pommereau and Goutail (1988) following the discovery of the O_3 hole in Antarctica by Farman et al. (1985). Since the late 80's, about twenty instruments distributed in latitude have been deployed within the Network for the Detection of Atmospheric Composition Change (NDACC). The SAOZ TOC measurements are performed in the visible Chappuis bands between 450 and 550 nm with a spectral resolution of 1.0 nm, twice a day, at sunrise and sunset at solar zenith angle between 86 and 91°. The retrieval makes use of the Differential Optical Absorption Spectroscopy (DOAS) procedure (Platt, 1994). SAOZ performances have been continuously evaluated by regular comparisons with UV-vis independent observations (e.g. Hofmann et al., 1995; Roscoe et al., 1999; Hendrick et al., 2011).

In this study, eight SAOZ stations deployed at all latitudes from the Arctic to the Antarctic (see Table 3 for their locations) have been used for IASI TOC validation. Collocated daytime (nighttime) IASI and sunrise (sunset) SAOZ measurements in a 300 km diameter semi-circular area located to the East (West) of the ground-based station are used for the comparisons. Note that similar results are found for day- and nighttime measurements, so only the results related to day time data are shown here.

Figure 11 shows the temporal variation of the monthly mean relative differences between IASI-A in blue and IASI-B in red against SAOZ day time TOCs for the eight SAOZ stations for the period 2008-2014. The relative difference is calculated as 100 x (IASI–SAOZ) / SAOZ. Here again, we clearly see the systematic overestimation of IASI TOCs from FORLI and the seasonality in the differences, both of increasing amplitude with latitude. Compared to SAOZ, the IASI TOCs are overestimated by 2-4% (1-2% dispersion) in the tropics and mid-latitudes, and bias and noise are increasing to about 7±3% at the polar circle, and to 15-20±15% at higher latitude (not shown). Table 4 gives a summary of the statistic by latitude zones. The mean biases, which varies also with the station, are attributed to i) the inconsistency between O_3 absorption cross-sections in the IR compared to the UV-vis (Picquet-Varrault et al., 2005; Gratien et al., 2010); ii) the reduced IASI sensitivity at high latitudes due to low brightness temperatures, especially in the winter because of ice surfaces; iii) the temperature profiles used in FORLI that are less reliable in the Southern high latitudes (August et al., 2012); and iv) the longitudinal variation of the O_3 profile ignored in SAOZ retrievals. In particular, the 4% bias drop between Reunion and Bauru stations located at the same latitude (see Fig. 11) is attributed to the larger O_3 concentration in the upper troposphere above the South American continent in contrast to the Indian Ocean (Pastel et al., 2014).

5 Validation of IASI ozone vertical profiles

In situ measurements of vertical O_3 profiles are routinely performed from balloon sondes launched at different stations around the world. The sondes provide measurements of O_3, temperature, pressure and humidity up to 30-35 km with a vertical resolution of ~150 m. For the validation of IASI O_3 vertical profiles, global profiles measured from 2008 to 2014 and archived at the WOUDC were extracted. Only sonde measurements based on electrochemical concentration cells (ECC), which measure the oxidation of a potassium iodine (KI) solution by O_3 (Komhyr et al., 1995), are used in this study. Their accuracy is generally sufficient (±5%) (Deshler et al., 2008; Smit et al., 2007) and they have been widely used before for the validation of satellite O_3 profiles (e.g. Nassar et al., 2008; Boynard et al., 2009; Keim et al., 2009; Kroon et al., 2011; Dufour et al., 2012; Verstraten et al., 2013).

We set the coincidence criteria between IASI and the sondes to a 50 km search radius between the satellite centre of pixel and the geocolocation of the ground-based station as well as to a temporal coincidence of ±10 h. We chose these two collocation criteria in order to obtain a sufficient number of data pairs in the tropics and the Southern mid-latitudes for statistical comparison. 57 ozonesonde stations in mid-latitudes, polar and tropical regions were considered for the comparison. Figure 12 (left panel) presents a map of the ozonesonde stations used in the validation exercise, showing that most of sonde stations used in this study are located in the Northern mid-latitudes. Figure 12 (right panel) shows the distribution of the amount of IASI-ozonesonde coincidences available for this study as a function of latitude. More than 7600 sonde measurements and 77000 coincident clear-sky IASI observations during a period extending from January 2008 to December 2014 were found with more than half of them located in the Northern mid-latitudes.

To allow for a meaningful comparison with the high vertical resolution profiles measured by ozonesondes, the difference in vertical resolution and sensitivity between the two data sets has to be accounted for. The ozonesonde vertical profiles were smoothed according to the IASI averaging kernel and *a priori* constraints leading to a vertical profile representing what IASI would measure for the same sonde sampled atmospheric air mass. According to Rodgers (2000) the smoothing of the true state can be characterized as follows :

$$\boldsymbol{x}_s = \boldsymbol{x}_a + \mathbf{A}(\boldsymbol{x}_{sonde} - \boldsymbol{x}_a) \tag{1}$$

where $\boldsymbol{x}_s$ is the smoothed ozonesonde profile, $\boldsymbol{x}_{sonde}$ is the measured ozonesonde profile, $\boldsymbol{x}_a$ is the *a priori* profile and $\mathbf{A}$ the averaging kernel matrix.

Figure 13 shows the comparison between the mean retrieved IASI-A profile with the smoothed and raw ozonesonde profiles for different latitude bands taking into account all IASI-A-sonde coincidences within the seven-year (2008-2014) period. The relative difference (100 x (IASI – sonde) / sonde) between the retrieved profile and the smoothed (blue) and the raw (green) ozonesonde profiles is also displayed. In the mid-latitudes, the relative difference between the retrieved and smoothed ozonesonde profile is generally smaller than that between the retrieved and the raw ozonesonde profile. This is due to the smoothing error that arises when applying the IASI averaging kernels to the ozonesonde profiles according to Eq. (1), which partly removes the systematic differences. In the tropics and at high latitudes, the relative difference between the retrieved

Atmospheric
Measurement
Techniques
Discussions

and the smoothed ozonesonde profile can be larger than that between the retrieved and the raw ozonesonde profile, especially in the UTLS region. In the following, we discuss the comparison with the smoothed ozonesonde profiles and partial columns only. The two main features of the comparison between IASI and sonde O_3 mixing ratios are that (1) IASI generally underestimates O_3 in the troposphere (up to 15% in the mid-latitudes) and overestimates O_3 in the stratosphere (up

5   to 40% in the tropical upper stratosphere) and (2) for all latitude bands except for the Northern mid-latitudes, the bias is larger in the UTLS region (up to ±50% in the tropics). In the tropics, large negative and positive biases are found in the UT and the LS, respectively. This can be explained by the low O_3 amounts leading to larger relative errors (Wespes et al., 2015). Another possible reason can be the vertical sampling that is not high enough in the tropopause region or the *a priori* profile used in FORLI-O3 v20140922 that is not latitudinal dependent. In the upper stratosphere (above 30 hPa/25 km), IASI is

10   generally biased positively by 10 to 40%, suggesting that the bias found for the TOC (see previous sections) is linked to the bias found in the upper stratosphere.

A detailed statistic comparison between IASI and sonde O_3 partial columns was performed for four vertical layers as defined in Section 2: surface-300 hPa, 300-150 hPa, 150-25 hPa and 25-3 hPa respectively (see Table 5). In the troposphere, a better agreement between IASI and sonde O_3 is found for the tropics (R=0.71-0.80) than for the mid-latitude regions

15   (R=0.47-0.58). This is due to the fact that IASI retrievals are more sensitive to tropospheric O_3 in the tropics generally characterized by a higher surface temperature. The better agreement between IASI and sonde O_3 is found for the 150-25 hPa partial columns with correlation coefficients ranging from 0.76 to 0.88 (except for the tropics). This is due to the fact that IASI is generally more sensitive to O_3 in this part of the atmosphere as shown by the averaging kernel functions plotted in Fig. 2. Note that the low bias found in the UTLS region (corresponding to the 300-150 partial column) and reported in

20   Table 5 has to be taken with care since IASI is negatively biased in the upper troposphere and positively bias in the lower stratosphere as shown in Fig. 13. For the 150-25 hPa and the 25-3 hPa layers, IASI systematically overestimates ozone, with values generally ranging from 5 to 30%.

A statistical comparison between IASI-A and IASI-B against sonde O_3 partial columns was performed for the period 2013-2014 in the midlatitudes where most of ozonesonde measurements are found. Figure 14 shows the relative difference, the

25   RMS and the correlation coefficient calculated for each season for the TROPO, UTLS, MS and US partial columns. The first thing to note is that there is an excellent agreement between the IASI-A and IASI-B seasonal variability when compared to ozonesonde measurements. We clearly see that both sensors underestimate O_3 in the troposphere with the largest bias/lowest correlation found in summer and the lowest bias/largest correlation in winter. This can be explained by the fact that in summer the higher photochemical activity leads to higher O_3 concentrations, in particular a more pronounced diurnal cycle.

30   The summer O_3 values will change more in 50 min (which is the delay between the two sensors) than in winter and hence the difference is more pronounced in summer than it is in winter. Another apparent feature is that both sensors overestimate O_3 in the stratosphere with the largest bias in the upper stratosphere, especially in spring (bias ~27%).

6 Towards a decrease in the bias

In order to compute new products related to radiative forcing studies (Doniki et al., 2015), new developments were made in the FORLI-O3 retrieval software. Look-up tables (LUTs) were recalculated to cover a larger spectral range (960 – 1105 cm^{-1}) using the HITRAN 2012 spectroscopic database (Rothman et al., 2013) instead of the HITRAN 2004 database (Rothman

5 et al., 2005) and correcting numerical implementation, especially with regard to the LUTs at higher altitude. Here we assess the new FORLI-O3 retrievals performed for 12 days (the 15th of each month) in 2011. In the following the updated version of FORLI-O3 is called v20151001, and the relative difference between both versions of FORLI-O3 is calculatd as 100 x (v20140922-v20151001) / v20151001 (%). Only common pixels of IASI-A were used for the comparison between the two versions of FORLI-O3.

10 The current version of the HITRAN database between 960 and 1105 cm^{-1} includes 52970 O_3 entries of five isotopologues. The line lists of two databases HITRAN 2012 and HITRAN 2004 differ by 15 transitions of very weak hot band $n_1+2n_2+n_3-2n_2-n_3$ in the mentioned above spectral range. The line positions and line intensities of all other transitions are identical in both lists. The difference between the two data sets is in the broadening parameters (g_{air} and g_{self}) and in temperature-dependent exponent coefficient n for g_{air}. The actual values of the g_{air}, g_{self} and n parameters in the HITRAN 2012 database

15 are based on the results of Wagner et al. (2002).

Figure 15 shows the global relative differences of TOC obtained between FORLI-O3 v20140922 and v20151001 for the 15th of each month of 2011 for day time and nighttime measurements separately. The data were averaged over a 1°x1° grid. The relative differences between both versions of FORLI-O3 range between 3 and 6% depending on month and observation time. With FORLI-O3 v20151001, there is evidence that retrieved total O_3 columns are lower by 3 – 6% and that this will

20 lead to a marked improvement of the comparison with UV-vis measurements.

In order to investigate the altitude/pressure range impacted by the changes in FORLI-O3, Fig. 16 shows the vertical profiles of relative difference between FORLI-O3 v20140922 and FORLI-O3 v20151001 along with the standard deviation averaged over the 12 days of 2011 for different latitude bands and day time measurements. FORLI-O3 v20151001 gives lower concentrations of O_3 in the upper stratosphere (above 30 hPa/25 km) but higher concentrations in UTLS region. In the upper

25 stratosphere, the differences vary as a function of latitude: the largest differences are found at high latitudes (up to 20%) and the lowest differences are found in the tropics (less than 10%). In the lower troposphere the differences between both versions of FORLI-O3 are smaller (< 5%). This suggests that the changes made in FORLI v20151001 will impact more the upper stratosphere where most of O_3 is located than the UTLS characterized by lower amount of O_3. Similar results are found for nighttime measurements (not shown here).

30 Total O_3 columns obtained from FORLI-O3 v20151001 were compared to GOME-2A data for the 12 days of 2011. Data (day time only) were averaged over a 1° x 1° grid. Figure 17 shows the global distribution of the relative difference of TOCs between FORLI-O3 v20140922 (left panel) and v20151001 (right panel) against GOME-2A data. Overall, a much better agreement between IASI-A and GOME-2A is found when FORLI-O3 v20151001 is used although local differences still

remain especially in the Antarctic region. The global mean bias found between FORLI-O3 v20140922 and FORLI-I3 v20151001 against and GOME-2A TOCs decreases from 6.5±7.3% to 2.1±9.0%.

We also compared both versions of FORLI-O3 to Brewer and Dobson ground-based measurements. The colocation criteria are the same as that described in Section 4.2. Figure 18 shows the latitudinal comparisons between FORLI-O3 v20140922 in blue and FORLI-O3 v20151001 in magenta against Brewer, on the right, and Dobson, on the left, TOCs for the 12 days of 2011. The Brewer vs FORLI-O3 v20151001 comparisons revolve around the 0% difference line for all Northern latitudes. The Dobson FORLI-O3 v20151001 comparisons show a peak-to-peak variability between 0 and 4%, except in the Antarctic region. However, the Antarctic comparisons have also improved in v20151001 with a decrease of the bias from ~20% to around ~12%. The seasonal dependency and the daily timeseries (not shown here) also result in a uniform decrease of the differences between IASI and ground-based TOCs. For the 850 Brewer colocations (located mainly in the NH) mean differences decrease from 4.0±6.5% to 0.1±6.6% while for the 340 common Dobson daily values an improvement from 6.9±8.6% to 3.0±8.5% is found. The standard deviations remain unchanged between the two versions.

In order to check for improvement in stratosphere retrievals, we finally compared FORLI-O3 v20140922 and v20151001 to ozonesonde vertical profiles smoothed with the IASI averaging kernels. The colocation criterion is the same as that described in Section 5; it unfortunately leads to no colocation in the Southern mid-latitudes. A total of 29 sonde measurements and 449 coincident clear-sky IASI-A observations for the 12 days of 2011 were found in the NH. Figure 19 presents the vertical profiles of the relative differences between FORLI-O3 v20140922 (in blue) and v20151001 (in magenta) against ozonesonde measurements averaged over the 12 days of 2011 for different latitude bands. For all latitudes except the Northern high latitudes, we can see an improvement in the upper stratosphere (above 30 hPa/25 km) with FORLI-O3 v20151001 (the bias decreases by ~5-10% depending on the latitudes). In the UTLS region, the differences between FORLI-O3 v20151001 and sonde O_3 concentrations are larger for all latitudes. However the O_3 amount being much lower in the UTLS than in the upper stratosphere, this does not affect the retrieved total O_3 column. No improvement is found in the troposphere.

These preliminary results show that the improvement in the retrieved IASI TOCs from FORLI v20151001 is mostly related to the improvement in retrieved O_3 in the upper stratosphere above 30 hPa/25 km.

7 Summary and conclusions

IASI-A and IASI-B O_3 (total and vertical profiles) data retrieved with the FORLI v20140922 software were validated against independent observations during the period 2008-2014, on a global scale. For the validation of TOCs, a direct comparison of IASI data with GOME-2, Brewer and Dobson spectrophotometers and SAOZ spectrometer data was performed. For the validation of O_3 vertical profiles against ozonesonde measurements, the ozonesonde vertical profiles were smoothed according to the IASI averaging kernel and *a priori* constraints, which leads to a vertical profile representing what IASI would measure for the same sonde sampled atmospheric air mass. The main findings of this validation exercise can be summarized as follow:

Atmospheric
Measurement
Techniques
Discussions

1. The consistency between IASI-A and IASI-B TOCs (day- and night- time) has been investigated for the period 2013-2014, and both products are consistent with differences generally less than 1% irrespective the latitude. A global difference of only 0.2±0.8% was found, with IASI-B providing slightly lower values. The comparison between IASI-A and IASI-B O_3 vertical profiles showed differences within 2% for the entire altitude range for all latitudes. IASI-A tends to measure more O_3 in the stratosphere and less O_3 in the troposphere compared to IASI-B. Both instruments agree best above 20 km, where most of O_3 is located (differences less than 0.5%). In the troposphere, the mean difference between IASI-A and IASI-B O_3 is larger (2.0±0.2%). Possible reasons for the differences found are the ~50 min temporal shift and the different geometry of observations between both sensors.

2. Globally, IASI with FORLI processing overestimates GOME-2 TOCs by ~6.2±7.5%, with a clear latitudinal and seasonal dependence. The lowest differences are found in the middle latitudes and the tropics (4-6%) while the largest differences are found at high latitudes, especially over Antarctica (11-15% depending on the season). The comparison with Brewer and Dobson spectrophotometer TOCs shows that a near-constant IASI overestimation of around 5% is found for all latitudes and for both types of ground-based observations with the exception of the high latitudes where the difference to both the Dobson and Brewer TOCs rises to 9% and 20% in the Arctic and Antarctic region, respectively. The comparison with SAOZ measurements shows a mean bias between IASI and SAOZ TOCs of 2-4% in the middle latitudes and tropics, and 7% at the polar circle (60°N-70°N). The larger differences found at high latitudes are attributed to reduced IASI sensitivity associated with high latitudes (low brightness temperature) and the temperature profiles used in FORLI that are less reliable in Antarctica.

3. The comparison with ozonesonde vertical profiles shows that the relative differences vary as a function of the altitude. In the troposphere, IASI generally underestimates O_3 by up to 15% except over the Antarctic region. In the lower/middle stratosphere IASI overestimates O_3 and the largest differences are found in the tropical tropopause region (~16 km), which can be explained by the low O_3 amounts leading to larger relative error. Part of the discrepancies can also be attributed to the *a priori* O_3 profile used in FORLI-O3, which is not latitudinal dependent. In the upper stratosphere, IASI-A is positively biased by 10-40% depending on the latitude zone. In the Northern middle latitudes, the bias varies within ±20% for the entire altitude range. A detailed comparison performed for different partial columns shows a better agreement between IASI and sonde tropospheric O_3 for the tropics (R>0.71-0.80) than for the mid-latitude regions (R=0.47-0.58), which is due to the fact that IASI retrievals are more sensitive to tropospheric O_3 in the tropics, which are generally characterized by higher surface temperature. A clear positive bias is found for the 25-3 hPa partial column, demonstrating that the systematic bias found for the TOCs is related to the bias in the upper stratosphere, where most of O_3 is located.

4. The FORLI retrieval software has been updated with LUTs recalculated to cover a larger spectral range (960 – 1105 cm^{-1}) using HITRAN 2012 spectroscopy database instead of HITRAN 2004, and correcting numerical implementation, especially with regard to the LUTs at higher altitude. The assessement of the updated version of FORLI-O3 (v20151001) shows a decrease in the IASI TOC bias by ~4%, bringing the overall global discrepancy to

Atmospheric
Measurement
Techniques
Discussions

~1-2% on average. The comparison between IASI and sonde O_3 vertical profiles confirms that the improvement is mainly located in the stratosphere, above 20 km. A smaller bias in the UTLS and the troposphere remains. Possible explanation of the bias in the UTLS could be the use of rough vertical sampling in the part of the atmosphere (each kilometer) or the use of a not latitudinal dependent *a priori* profile. Detailed investigations on the retrievals

5   processing need to be performed.

The operationnal IASI O_3 products (total and vertical profiles) starting in October 2007 are generated by the LATMOS and ULB in a near-real time mode. FORLI-O3 v20140922 products are already part of the EUMETSAT's O3M-SAF Official Validation Monitoring found in lap3.physics.auth.gr/eumetsat/ as part of the operational EUMETSAT services. As FORLI-O3 v20151001 is shown to give a more accurate O_3 product than FORLI-O3 v20140922, the data record is currently being

10   back and forward processed for the entire period of IASI (2007-present). The updated FORLI v20151001 will also be implemented into the EUMETSAT processing environment and the new products should be distributed by EumetCast in 2016.

References

25   Antón, M., Loyola, D., Clerbaux, C., López, M., Vilaplana, J. M., Bañón, M., Hadji-Lazaro, J., Valks, P., Hao, N., Zimmer, W., Coheur, P. F., Hurtmans, D., and Alados-Arboledas, L.: Validation of the MetOp-A total ozone data from GOME-2 and IASI using reference ground-based measurements at the Iberian Peninsula, Remote Sens. Environ., 115, 1380–1386, 2011.

August, T., Klaes, D., Schlüssel, P., Hultberg, T., Crapeau, M., Arriaga, A., O'Carroll, A., Coppens, D., Munro, R., and Calbet, X.: IASI on Metop-A: Operational Level 2 retrievals after five years in orbit, J. Quant. Spectrosc. Ra., 113, 1340–

30   1371, doi: 10.1016/j.jqsrt.2012.02.028, 2012.

Atmospheric
Measurement
Techniques
Discussions

Balis, D., Kroon, M., Koukouli, M. E., Labow, G., Veefkind, J. P., and McPeters, R. D.: Validation of Ozone Monitoring Instrument total ozone column measurements using Brewer and Dobson spectrophotometer ground based observations, J. Geophys. Res., 112, D24S46, doi:10.1029/2007JD008796, 2007a.

Balis, D., Lambert, J.-C., Van Roozendael, M., Spurr, R., Loyola, D., Livschitz, Y., Valks, P., Amiridis, V., Gerard, P.,
5   Granville, J., and Zehner, C.: Ten years of GOME/ERS2 total ozone data the new GOME data processor (GDP) version 4: 2. Ground-based validation and comparisons with TOMS V7/V8, J. Geophys. Res., 112, D07307, doi: 10.1029/2005JD00637, 2007b.

Boynard, A., Clerbaux, C., Coheur, P.-F., Hurtmans, D., Turquety, S., George, M., Hadji-Lazaro, J., Keim, C., and Meyer-Arnek, J.: Measurements of total and tropospheric ozone from IASI: comparison with correlative satellite, ground-based and
10   ozonesonde observations, Atmos. Chem. Phys., 9, 6255–6271, doi:10.5194/acp-9-6255-2009, 2009.

Boynard, B., Clerbaux, C., Clarisse, L., Safieddine, S., Pommier, M., van Damme, M., Bauduin, S., Oudot, C., Hadji-Lazaro, J., Hurtmans, D., and Coheur, P-F.: First simultaneous space measurements of atmospheric pollutants in the boundary layer from IASI: a case study in the North China Plain. Geophys. Res. Letters., http://onlinelibrary.wiley.com/doi/10.1002/2013GL058333/abstract, 2014.

15   Brunekreef, B., and Holgate, S. T.: Air pollution and health, Lancet, 360, 1233–1242, doi:10.1016/S0140-6736(02)11274-8, 2002.

Chameides, W. L. and Walker, J. C. G.: A photochemical theory for tropospheric ozone, J. Geophys. Res., 78, 8751–8760, 1973.

Clerbaux, C., Boynard, A., Clarisse, L., George, M., Hadji-Lazaro, J., Herbin, H., Hurtmans, D., Pommier, M., Razavi, A.,
20   Turquety, S., Wespes, C., and Coheur, P.-F.: Monitoring of atmospheric composition using the thermal infrared IASI/MetOp sounder, Atmos. Chem. Phys., 9, 6041-6054, doi:10.5194/acp-9-6041-2009, 2009.

Clerbaux, C., Hadji-Lazaro, J., Turquety, S., George, M., Boynard, A., Pommier, M., Safieddine, S. Coheur, P.-F., Hurtmans, D., Clarisse, L., and Van Damme, M., Tracking pollutants from space: Eight years of IASI satellite observation, Comptes Rendus Geoscience, http://dx.doi.org/10.1016/j.crte.2015.06.001, 2015.

25   Crutzen, P. J.: Photochemical reactions initiated by and influencing ozone in the unpolluted troposphere, Tellus, 26, 47–57, 1973.

Deshler, T., Mercer, J. L., Smit, H. G. J., Stubi, R., Levrat, G., Johnson, B. J., Oltmans, S. J., Kivi, R., Thompson, A. M., Witte, J., Davies, J., Schmidlin, F. J., Brothers, G., and Sasaki, T.: Atmospheric comparison of electrochemical cell ozonesondes from different manufacturers, and with different cathode solution strengths: The Balloon Experiment on
30   Standards for Ozonesondes, J. Geophys. Res., 113, D04307, doi:10.1029/2007JD008975, 2008.

Dessler, A.: Chemistry and Physics of Stratospheric Ozone, International Geophysics Series, vol. 74, Academic Press, London, San Diego, 2000.

Doniki, S., Hurtmans, D., Clarisse, L., Clerbaux, C., Worden, H. M., Bowman, K. W., and Coheur, P.-F.: Instantaneous longwave radiative impact of ozone: an application on IASI/MetOp observations, Atmos. Chem. Phys., 15, 12971-12987, doi:10.5194/acp-15-12971-2015, 2015.

Dufour, G., Eremenko, M., Orphal, J., and Flaud, J.-M.: IASI observations of seasonal and day-to-day variations of

5   tropospheric ozone over three highly populated areas of China: Beijing, Shanghai, and Hong Kong, Atmos. Chem. Phys., 10, 3787-3801, doi:10.5194/acp-10-3787-2010, 2010.

Dufour, G., Eremenko, M., Griesfeller, A., Barret, B., LeFlochmoën, E., Clerbaux, C., Hadji-Lazaro, J., Coheur, P.-F., and Hurtmans, D.: Validation of three different scientific ozone products retrieved from IASI spectra using ozonesondes, Atmos. Meas. Tech., 5, 611-630, doi:10.5194/amt-5-611-2012, 2012.

10   Dufour, G., Eremenko, M., Cuesta, J., Doche, C., Foret, G., Beekmann, M., Cheiney, A., Wang, Y., Cai, Z., Liu, Y., Takigawa, M., Kanaya, Y., and Flaud, J.-M.: Springtime daily variations in lower-tropospheric ozone over east Asia: the role of cyclonic activity and pollution as observed from space with IASI, Atmos. Chem. Phys., 15, 10839-10856, doi:10.5194/acp-15-10839-2015, 2015.

Eremenko, M., Dufour, G., Foret, G., Keim, C., Orphal, J., Beekmann, M., Bergametti, G., and Flaud, J.-M.: Tropospheric

15   ozone distributions over Europe during the heat wave in July 2007 observed from infrared nadir spectra recorded by IASI, Geophys. Res. Lett., 35, L18805, doi:10.1029/2008GL034803, 2008.

Farman, J. C., Gardiner, B.G., and Shanklin, J.D. : Large losses of total ozone in Antarctica reveal seasonal ClOx/NOx interaction, Nature, 315, 207-210, 1985.

Fioletov, V. E., Labow, G., Evans, R., Hare, E. W., Köhler, U., McElroy, C. T., Miyagawa, K., Redondas, A., Savastiouk,V.,

20   Shalamyansky, A. M., Staehelin, J., Vanicek, K., and Weber, M.: The performance of the ground-based total ozone network assessed using satellite data, J. Geophys. Res., 113, D14313, doi:10.1029/2008JD009809, 2008.

Fiore, A. M., Jacob, D. J., Bey, I., Yantosca, R. M., Field, B. D., Fusco, A. C., and Wilkinson, J. G.: Background ozone over the United States in summer: Origin, trend, and contribution to pollution episodes, J. Geophys. Res., 107(D15), 4275, doi:10.1029/2001JD000982, 2002.

25   Fishman, J. and Larsen, J. C.: Distribution of total ozone and stratospheric ozone in the tropics: Implications for the distribution of tropospheric ozone, J. Geophys. Res., 92, 6627–6634, 1987.

Fishman, J., Watson, C. E., Larsen, J. C., and Logan, J. A.: Distribution of tropospheric ozone determined from satellite data, J. Geophys. Res., 95, 3599–3617, 1990.

Fowler, D., Pilegaard, K., Sutton, M. A., Ambus, P., Raivonen, M., Duyzer, J., Simpson, D., Fagerli, H., et al.: Atmospheric

30   composition   change: Ecosystems-Atmosphere   interactions,   Atmos.   Environ.,   43,   5193–5267, doi:10.1016/j.atmosenv.2009.07.068, 2009.

Gazeaux, J., Clerbaux, C., George, M., Hadji-Lazaro, J., Kuttippurath, J., Coheur, P.-F., Hurtmans, D., Deshler, T., Kovilakam, M., Campbell, P., Guidard, V., Rabier, F., and Thépaut, J.-N.: Intercomparison of polar ozone profiles by

IASI/MetOp sounder with 2010 Concordiasi ozonesonde observations, Atmos. Meas. Tech., 6, 613-620, doi:10.5194/amt-6-613-2013, 2013.

Gratien, A., Picquet-Varrault, B., Orphal, J., Doussin, J.-F., and Flaud, J.-M.: New Laboratory Intercomparison of the Ozone Absorption Coefficients in the Mid-infrared (10 μm) and Ultraviolet (300-350 nm) Spectral Regions, Phys. Chem. A, 114,

5   10045–10048, 2010.

Hao, N., Koukouli, M. E., Inness, A., Valks, P., Loyola, D. G., Zimmer, W., Balis, D. S., Zyrichidou, I., Van Roozendael, M., Lerot, C., and Spurr, R. J. D.: GOME-2 total ozone columns from MetOp-A/MetOp-B and assimilation in the MACC system, Atmos. Meas. Tech., 7, 2937-2951, doi:10.5194/amt-7-2937-2014, 2014.

Hassinen, S., Balis, D., Bauer, H., Begoin, M., Delcloo, A., Eleftheratos, K., Gimeno Garcia, S., Granville, J., Grossi, M.,

10 Hao, N., Hedelt, P., Hendrick, F., Hess, M., Heue, K.-P., Hovila, J., Jønch-Sørensen, H., Kalakoski, N., Kiemle, S., Kins, L., Koukouli, M. E., Kujanpää, J., Lambert, J.-C., Lerot, C., Loyola, D., Määttä, A., Pedergnana, M., Pinardi, G., Romahn, F., van Roozendael, M., Lutz, R., De Smedt, I., Stammes, P., Steinbrecht, W., Tamminen, J., Theys, N., Tilstra, L. G., Tuinder, O. N. E., Valks, P., Zerefos, C., Zimmer, W., and Zyrichidou, I.: Overview of the O3M SAF GOME-2 operational atmospheric composition and UV radiation data products and data availability, Atmos. Meas. Tech. Discuss., 8, 6993-7056,

15 doi:10.5194/amtd-8-6993-2015, 2015.

Hendrick, F., Pommereau, J.-P., Goutail, F., Evans, R. D., Ionov, D., Pazmino, A., Kyrö, E., Held, G., Eriksen, P., Dorokhov, V., Gil, M., and Van Roozendael, M.: NDACC/SAOZ UV-visible total ozone measurements: improved retrieval and comparison with correlative ground-based and satellite observations, Atmos. Chem. Phys., 11, 5975-5995, doi:10.5194/acp-11-5975-2011, 2011.

20 Hofmann, D. J., Bonasoni, P., De Maziere, M., Evangelisti, F., Giovanelli, G., Glodman, A., Goutail, F., Harder, J., et al.: Intercomparison of UV/visible spectrometers for measurements of stratospheric NO2 for the Network for the Detection of Stratospheric Change, J. Geophys. Res., 100, 16,765-16,791, 1995.

Holton, J. R., Haynes, P. H., McIntyre, M. E., Douglass, A. R., Rood, R. B., and Pfister, L.: Stratosphere-troposphere exchange. Rev. Geophys., 33, 403–439, 1995.

25 HTAP: Hemispheric Transport of Air Pollution, UNECE, Geneva, 2010.

Hurtmans, D., Coheur, P.-F., Wespes, C., Clarisse, L., Scharf, O., Clerbaux, C., Hadji-Lazaro, J., George, M., and Turquety, S.: FORLI radiative transfer and retrieval code for IASI, J. Quant. Spectrosc. Ra., 113, 1391–1408, doi:10.1016/j.jqsrt.2012.02.036, 2012.

IPCC: Climate Change 2013: The Physical Science Basis: Summary for Policymakers, Cambridge, UK, 2013.

30 Jones, D. B. A., Bowman, K. W., Horowitz, L. W., Thompson, A. M., Tarasick, D. W., and Witte, J. C.: Estimating the summertime tropospheric ozone distribution over North America through assimilation of observations from the Tropospheric Emission Spectrometer, J. Geophys. Res., 113, D18307, doi:10.1029/2007JD009341, 2008.

Keim, C., Eremenko, M., Orphal, J., Dufour, G., Flaud, J.-M., Höpfner, M., Boynard, A., Clerbaux, C., Payan, S., Coheur, P.-F., Hurtmans, D., Claude, H., Dier, H., Johnson, B., Kelder, H., Kivi, R., Koide, T., López Bartolomé, M.,

Lambkin, K., Moore, D., Schmidlin, F. J., and Stübi, R.: Tropospheric ozone from IASI: comparison of different inversion algorithms and validation with ozone sondes in the northern middle latitudes, Atmos. Chem. Phys., 9, 9329-9347, doi:10.5194/acp-9-9329-2009, 2009.

Kerr, J. B.: New methodology for deriving total ozone and other atmospheric variables from Brewer spectrophotometer direct sun spectra, J. Geophys. Res., 107, 4731, doi:10.1029/2001JD001227, 2002.

Kerr, J. B., McElroy, C. T., Wardle, D. I., Olafson, R. A., and Evans, W. F. J.: The automated brewer spectrophotometer, in: Proc. Of the Quadrennial Ozone Symposium, Zerefos, C. S. and Ghazi, A. (Eds), pp. 611–614, D. Reidel Publ. Co., Dordrecht, 1984.

Komhyr, W. D. , Barnes, R. A., Brothers, G. B., Lathrop, J. A., and Opperman, D. P.: Electrochemical concentration cell ozonesonde performance evaluation during STOIC 1989, J. Geophys. Res., 100, 9231–9244, doi:10.1029/94JD02175, 1995.

Koukouli, M. E., Balis, D. S., Loyola, D., Valks, P., Zimmer, W., Hao, N., Lambert, J.-C., Van Roozendael, M., Lerot, C., and Spurr, R. J. D.: Geophysical validation and long-term consistency between GOME-2/MetOp-A total ozone column and measurements from the sensors GOME/ERS-2, SCIAMACHY/ENVISAT and OMI/Aura, Atmos. Meas. Tech., 5, 2169-2181, doi:10.5194/amt-5-2169-2012, 2012.

Koukouli, M. E., Lerot, C., Granville, J., Goutail, F., Lambert, J.-C., Pommereau, J.-P., Balis, D., Zyrichidou, I., et al.: Evaluating a new homogeneous total ozone climate data record from GOME/ERS-2, SCIAMACHY/Envisat, and GOME-2/MetOp-A, J. Geophys. Res. Atmos., 120, doi:10.1002/2015JD023699, 2015.

Kroon, M., de Haan, J. F., Veefkind, J. P., Froidevaux, L., Wang, R. Kivi, R., and Hakkarainen, J. J.: Validation of operational ozone profiles from the Ozone Monitoring Instrument, J. Geophys. Res., 116, D18305, doi:10.1029/2010JD015100, 2011.

Lerot, C., Van Roozendael, M., Spurr, R., Loyola, D., Coldewey-Egbers, M., Kochenova, S., van Gent, J., Koukouli, M., Balis, D., Lambert, J.-C., Granville, J. and Zehner, C.: Homogenized total ozone data records from the European sensors GOME/ERS-2, SCIAMACHY/Envisat, and GOME-2/MetOp-A, J. Geophys. Res. Atmos., 119(3), 1639–1662, doi:10.1002/2013JD020831, 2014.

Lim S. S., Vos T., Flaxman A. D., Danaei G., Shibuya K., Adair-Rohani H., Amann, M, Anderson, H. R., et al.: A comparative risk assessment of burden of disease and injury attributable to 67 risk factors and risk factor clusters in 21 regions, 1990–2010: a systematic analysis for the Global Burden of Disease study 2010, Lancet 380:2224–2260, 2012.

Loyola, D. G., Koukouli, M. E., Valks, P., Balis, D. S., Hao, N., Van Roozendael, M., Spurr, R. J. D., Zimmer, W., et al.: The GOME-2 total column ozone product: Retrieval algorithm and ground-based validation, J. Geophys. Res., 116, D07302, doi:10.1029/2010JD014675, 2011.

McPeters, R. D., Labow, G. J., and Logan, J. A.: Ozone climatological profiles for satellite retrieval algorithms, J. Geophys. Res., 112, D05308, doi:10.1029/2005JD006823, 2007.

Miles, G. M., Siddans, R., Kerridge, B. J., Latter, B. G., and Richards, N. A. D.: Tropospheric ozone and ozone profiles retrieved from GOME-2 and their validation, Atmos. Meas. Tech., 8, 385-398, doi:10.5194/amt-8-385-2015, 2015.

Atmospheric
Measurement
Techniques
Discussions

Monks, P. S., Archibald, A. T., Colette, A., Cooper, O., Coyle, M., Derwent, R., Fowler, D., Granier, C., Law, K. S., Mills, G. E., Stevenson, D. S., Tarasova, O., Thouret, V., von Schneidemesser, E., Sommariva, R., Wild, O., and Williams, M. L.: Tropospheric ozone and its precursors from the urban to the global scale from air quality to short-lived climate forcer, Atmos. Chem. Phys., 15, 8889-8973, doi:10.5194/acp-15-8889-2015, 2015.

5 Munro, R., Lang, R., Klaes, D., Poli, G., Retscher, C., Lindstrot, R., Huckle, R., Lacan, A., Grzegorski, M., Holdak, A., Kokhanovsky, A., Livschitz, J., and Eisinger, M.: The GOME-2 instrument on the Metop series of satellites: instrument design, calibration, and level 1 data processing – an overview, Atmos. Meas. Tech. Discuss., 8, 8645-8700, doi:10.5194/amtd-8-8645-2015, 2015.

Nassar, R., Logan, J. A., Worden, H. M., Megretskaia, I. A., Bowman, K. W., Osterman, G. B., Thompson, A. M., Tarasick, D. W., Austin, S., Claude, H., Dubey, M. K., Hocking, W. K., Johnson, B. J., Joseph, E., Merrill, J., Morris, G. A., Newchurch, M., Oltmans, S. J., Posny, F., Schmidlin, F. J., Vomel, H., Whiteman, D. N., and Witte, J. C.: Validation of Tropospheric Emission Spectrometer (TES) nadir ozone profiles using ozonesonde measurements, J. Geophys. Res.-Atmos., 113, D15S17, doi:10.1029/2007jd008819, 2008.

Oetjen, H., Payne, V. H., Kulawik, S. S., Eldering, A., Worden, J., Edwards, D. P., Francis, G. L., Worden, H. M., Clerbaux, C., Hadji-Lazaro, J., and Hurtmans, D.: Extending the satellite data record of tropospheric ozone profiles from Aura-TES to MetOp-IASI: characterisation of optimal estimation retrievals, Atmos. Meas. Tech., 7, 4223-4236, doi:10.5194/amt-7-4223-2014, 2014.

Pastel, M., Pommereau, J.-P., Goutail, F., Richter, A., Pazmiño, A., Ionov, D., and Portafaix, T.: Construction of merged satellite total O_3 and NO_2 time series in the tropics for trend studies and evaluation by comparison to NDACC SAOZ measurements, Atmos. Meas. Tech., 7, 3337-3354, doi:10.5194/amt-7-3337-2014, 2014.

Picquet-Varrault, B., Orphal., J., Doussin, J.-F., Carlier, P., and Flaud, J.-M.: Laboratory Intercomparison of the Ozone Absorption Coefficients in the Mid-infrared (10 µm) and Ultraviolet (300-350 nm) Spectral Regions, J. Phys. Chem. A, 109, 1008-1014, 2005.

Platt, U.: Differential optical absorption spectroscopy (DOAS), Chem. Anal. Series, 127, 27 - 83, 1994.

Pommereau, J.-P. and Goutail, F.: Ground-based measurements by visible spectrometry during Arctic Winter and Spring, Geophys. Res. Lett., 15, 891–894, 1988.

Pommier, M., Clerbaux, C., Law, K. S., Ancellet, G., Bernath, P., Coheur, P.-F., Hadji-Lazaro, J., Hurtmans, D., Nédélec, P., Paris, J.-D., Ravetta, F., Ryerson, T. B., Schlager, H., and Weinheimer, A. J.: Analysis of IASI tropospheric O3 data over the Arctic during POLARCAT campaigns in 2008, Atmos. Chem. Phys., 12, 7371-7389, doi:10.5194/acp-12-7371-2012, 2012.

30 Rodgers, C. D.: Inverse Methods for Atmospheric Sounding: Theory and Practice, World Scientific, Series on Atmospheric, Oceanic and Planetary Physics, 2, Hackensack, N. J., 2000.

Roscoe, H. K., Johnston, P. V., Van Roozendael, M., Richter, A., Sarkissian, A., Roscoe, J., Preston, K. E., Lambert, J.-C., Hermans, C., Decuyper, W., Dzienus, S., Winterrath, T., Burrows, J. P., Goutail, F., Pommereau, J.-P., D'Almeida, E., Hottier, J., Coureul, C., Didier, R., Pundt, I., Bartlett, L. M., McElroy, C. T., Kerr, J. E., Elokhov, A., Giovanelli, G.,

Atmospheric
Measurement
Techniques
Discussions

Ravegnani, F., Premuda, M., Kostadinov, I., Erle, F., Wagner, T., Pfeilsticker, K., Kenntner, M., Marquard, L. C., Gil, M., Puentedura, O., Yela, M., Arlander, D. W., Kastad Hoiskar, B. A., Tellefsen, C. W., Karlsen Tørnkvist, K., Heese, B., Jones, R. L., Aliwell, S. R., and Freshwater, R. A.: Slant column measurements of O3 and NO2 during the NDSC intercomparison of zenith-sky UV-visible spectrometers in June 1996, J. Atmos. Chem., 32, 281–314, 1999.

5 Rothman, L.S., Jacquemart, D., Barbe, A., Benner, D.C., Birk, M., Brown, L.R., Carleer, M.R., Chackerian, C., Jr., Chance, K., Coudert, L.H., Dana, V., Devi, V.M., Flaud, J.M., Gamache, R.R., Goldman, A., Hartmann, J.M., Jucks, K.W., Maki, A.G., Mandin, J.Y., Massie, S.T., Orphal, J., Perrin, A., Rinsland, C.P., Smith, M.A.H., Tennyson, J., Tolchenov, R.N., Vander Auwera, J., Varanasi, P., and Wagner, G.: The HITRAN2004 molecular spectroscopic database, J. Quant. Spectrosc. Ra., 96, 139-204, doi: 10.1016/j.jqsrt.2004.10.008, 2005.

10 Rothman, L., Gordon, I., Babikov, Y., Barbe, A., Benner, D. C., Bernath, P., Birk, M., Bizzocchi, L., Boudon, V., Brown, L., Campargue, A., Chance, K., Cohen, E., Coudert, L., Devi, V., Drouin, B., Fayt, A., Flaud, J.-M., Gamache, R., Harrison, J., Hartmann, J.-M., Hill, C., Hodges, J., Jacquemart, D., Jolly, A., Lamouroux, J., Roy, R. L., Li, G., Long, D., Lyulin, O., Mackie, C., Massie, S., Mikhailenko, S., Müller, H., Naumenko, O., Nikitin, A., Orphal, J., Perevalov, V., Perrin, A., Polovtseva, E., Richard, C., Smith, M., Starikova, E., Sung, K., Tashkun, S., Tennyson, J., Toon, G., Tyuterev, V., and

15 Wagner, G.: The HITRAN2012 molecular spectroscopic database, J. Quant. Spectrosc. Ra., 130, 4–50, doi: 10.1016/j.jqsrt.2013.07.002, 2013.

Safieddine, S., Clerbaux, C., George, M., Hadji-Lazaro, J., Hurtmans, D., Coheur, P.-F., Wespes, C., Layola, D., Valks, P. and Hao, N.: Tropospheric ozone and nitrogen dioxide measurements in urban and rural regions as seen by IASI and GOME-2. J. Geophys. Res., Atmospheres, VOL. 118, 1-12, http://onlinelibrary.wiley.com/doi/10.1002/jgrd.50669/abstract,

20 2013.

Safieddine, S., Boynard, A., Coheur, P.-F., Hurtmans, D., Pfister, G., Quennehen, B., Thomas, J. L., Raut, J.-C., Law, K. S., Klimont, Z., Hadji-Lazaro, J., George, M., and Clerbaux, C.: Summertime tropospheric ozone assessment over the Mediterranean region using the thermal infrared IASI/MetOp sounder and the WRF-Chem model, Atmos. Chem. Phys., 14, 10119-10131, doi:10.5194/acp-14-10119-2014, http://www.atmos-chem-phys.net/14/10119/2014/acp-14-10119-2014.html,

25 2014.

Safieddine, S., Boynard, A., Hao, N., Huang, F., Wang, L., Ji, D., Barret, B., Ghude, S. D., Coheur, P.-F., Hurtmans, D., and Clerbaux, C.: Tropospheric Ozone Variability during the East Asian Summer Monsoon as Observed by Satellite (IASI), Aircraft (MOZAIC) and Ground Stations, Atmos. Chem. Phys. Discuss., 15, 31925-31950, doi:10.5194/acpd-15-31925-2015, 2015.

30 Scannell, C., Hurtmans, D., Boynard, A., Hadji-Lazaro, J., George, M., Delcloo, A., Tuinder, O., Coheur, P.-F., and Clerbaux, C.: Antarctic ozone hole as observed by IASI/MetOp for 2008–2010, Atmos. Meas. Tech., 5, 123-139, doi:10.5194/amt-5-123-2012, 2012.

Shindell, D., Kuylenstierna, J. C. I., Vignati, E., van Dingenen, R., Amann, M., Klimont, Z., Anenberg, S. C., Muller, N., Janssens-Maenhout, G., Raes, F., Schwartz, J., Faluvegi, G., Pozzoli, L., Kupiainen, K., Höglund-Isaksson, L., Emberson,

Atmospheric
Measurement
Techniques
Open Access
EGU
Discussions

L., Streets, D., Ramanathan, V., Hicks, K., Oanh, N. T. K., Milly, G., Williams, M., Demkine, V., and Fowler, D.: Simultaneously Mitigating Near-Term Climate Change and Improving Human Health and Food Security, Science, 335, 183–189, doi:10.1126/science.1210026, 2012.

Smit, H. G. J., Straeter, W., Johnson, B., Oltmans, S., Davies, J., Tarasick, D. W., Hoegger, B., Stubi, R., Schmidlin, F., Northam, T., Thompson, A., Witte, J., Boyd, I., and Posny, F.: Assessment of the performance of ECC-ozonesondes under quasi-flight conditions in the environmental simulation chamber: Insights from the Juelich Ozone Sonde Intercomparison Experiement (JOSIE), J. Geophys. Res., 112, D19306, doi:10.1029/2006JD007308, 2007.

Stevenson, D. S., Dentener, F. J., Schultz, M. G., Ellingsen, K., van Noije, T. P. C., Wild, O., Zeng, G., Amann, M., Atherton, C. S., Bell, N., Bergmann, D. J., Bey, I., Butler, T., Cofala, J., Collins, W. J., Derwent, R. G., Doherty, R. M., Drevet, J., Eskes, H. J., Fiore, A. M., Gauss, M., Hauglustaine, D. A., Horowitz, L. W., Isaksen, I. S. A., Krol, M. C., Lamarque, J. F., Lawrence, M. G., Montanaro, V., Muller, J. F., Pitari, G., Prather, M. J., Pyle, J. A., Rast, S., Rodriguez, J. M., Sanderson, M. G., Savage, N. H., Shindell, D. T., Strahan, S. E., Sudo, K., and Szopa, S.: Multimodel ensemble simulations of present-day and near-future tropospheric ozone, J. Geophys. Res.-Atmos., 111, D08301, doi:10.1029/2005jd006338, 2006.

Toihir, A. M., Bencherif, H., Sivakumar, V., El Amraoui, L., Portafaix, T., and Mbatha, N.: Comparison of total column ozone obtained by the IASI-MetOp satellite with ground-based and OMI satellite observations in the southern tropics and subtropics, Ann. Geophys., 33, 1135-1146, doi:10.5194/angeo-33-1135-2015, 2015.

Valks, P., Hao, N., Gimeno Garcia, S., Loyola, D., Dameris, M., Jöckel, P., and Delcloo, A.: Tropical tropospheric ozone column retrieval for GOME-2, Atmos. Meas. Tech., 7, 2513–2530, doi:10.5194/amt-7-2513-2014, 2014.

Van Roozendael, M., Spurr, R., Loyola, D., Lerot, C., Balis, D., Lambert, J.-C., Zimmer, W., van Gent, J., van Geffen, J., Koukouli, M., Granville, J., Doicu, A., Fayt, C., and Zehner, C.: Sixteen years of GOME/ERS-2 total ozone data: The new direct-fitting GOME Data Processor (GDP) version 5 – Algorithm description, J. Geophys. Res., 117, D03305, doi: 10.1029/2011JD016471, 2012.

Verstraeten, W. W., Boersma, K. F., Zörner, J., Allaart, M. A. F., Bowman, K. W., and Worden, J. R.: Validation of six years of TES tropospheric ozone retrievals with ozonesonde measurements: implications for spatial patterns and temporal stability in the bias, Atmos. Meas. Tech., 6, 1413-1423, doi:10.5194/amt-6-1413-2013, 2013.

Verstraeten, W. W., Neu, J. L., Williams, J. E., Bowman, K. W., Worden, J. R., and Boersma, K. F.: Rapid increases in tropospheric ozone production and export from China, Nat. Geosci. 8, 690–695, doi:10.1038/ngeo2493, 2015.

Wagner, G., Birk, M., Schrier, F., and Flaud, J.-M.: Spectroscopic database for ozone in the fundamental spectral regions, J. Geophys. Res., 107(D22), doi:10.1029/2001JD000818, 2002.

Weber, M., Lamsal, L. N., Coldewey-Egbers, M., Bramstedt, K., and Burrows, J. P.: Pole-to-pole validation of GOME WFDOAS total ozone with groundbased data, Atmos. Chem. Phys., 5, 1341-1355, doi:10.5194/acp-5-1341-2005, 2005.

Wespes, C., Emmons, L., Edwards, D. P., Hannigan, J., Hurtmans, D., Saunois, M., Coheur, P.-F., Clerbaux, C., Coffey, M. T., Batchelor, R. L., Lindenmaier, R., Strong, K., Weinheimer, A. J., Nowak, J. B., Ryerson, T. B., Crounse, J. D., and

Atmospheric
Measurement
Techniques
Open Access
EGU
Discussions

Wennberg, P. O.: Analysis of ozone and nitric acid in spring and summer Arctic pollution using aircraft, ground-based, satellite observations and MOZART-4 model: source attribution and partitioning, Atmos. Chem. Phys., 12, 237-259, doi:10.5194/acp-12-237-2012, 2012.

Wespes, C., Coheur, P.-F., Emmons, L. K., Hurtmans, D., Safieddine, S., Clerbaux, C., and Edwards, D. P.: Ozone
5   variability in the troposphere and the stratosphere from the first six years of IASI observations (2008–2013), Atmos. Chem. Phys. Discuss., 15, 27575-27625, doi:10.5194/acpd-15-27575-2015, 2015.

Worden, H. M., Logan, J. A., Worden, J. R., Beer, R., Bowman, K., Clough, S. A., Eldering, A., Fisher, B. M., Gunson, M. R., Herman, R. L., Kulawik, S. S., Lampel, M. C., Luo, M., Megretskaia, I. A., Osterman, G. B., and Shephard, M. W.: Comparisons of Tropospheric Emission Spectrometer (TES) ozone profiles to ozonesondes: Methods and initial results, J.
10   Geophys. Res., 112, D03309, doi:10.1029/2006JD007258, 2007.

Worden, H. M., Bowman, K. W., Worden, J. R., Eldering, A., and Beer, R.: Satellite measurements of the clear-sky greenhouse effect from tropospheric ozone, Nat. Geosci., 1, 305–308, 2008.

Atmospheric
Measurement
Techniques
Open Access
Discussions
EGU

Tables

Table 1. Summary of the correlation (R), the bias and the standard deviation of IASI-A total ozone column retrieved from FORLI-O3 v20140922 relative to the O3M SAF GOME-2A retrievals, for each season of the period 2008-2014. The bias and the standard deviation are given in percent. The correlation coefficients higher than 0.85 are indicated in bold.

Latitude range	Dec-Jan-Feb		Mar-Apr-May		Jun-Jul-Aug		Sep-Oct-Nov	
	R	Bias (%)	R^2	Bias (%)	R^2	Bias (%)	R^2	Bias (%)
90°S–90°N	**0.93**	7.1±7.1	**0.95**	7.0±76.8	**0.95**	5.5±4.2	**0.98**	6.4±4.8
60–90°N	0.75	4.3±7.0	0.42	5.4±4.2	0.61	4.7±2.2	**0.92**	6.8±2.7
30–60°N	**0.98**	4.4±2.5	**0.97**	6.0±2.3	**0.95**	4.9±1.8	**0.96**	4.0±1.9
0–30°N	**0.88**	6.1±2.0	**0.93**	6.7±12.1	**0.87**	6.6±2.3	0.79	5.9±1.7
0–30°S	**0.91**	6.4±1.4	0.78	6.7±1.6	**0.91**	5.9±1.6	**0.96**	5.9±1.5
30–60°S	**0.99**	5.2±0.8	**0.97**	4.0±1.0	**0.93**	2.6±1.9	**0.99**	4.2±1.2
60–90°S	0.26	15.6±12.3	0.25	13.5±14.0	**0.88**	12.3±10.0	**0.96**	11.6±9.0

5

Atmospheric
Measurement
Techniques
Open Access
Discussions

EGU

Table 2: List of the 47 Brewer and 53 Dobson quality assured stations that contribute to the entire validation time period from 2008 to 2014 inclusive.

Brewer Station Name	Latitude (°)	Longitude (°)	Dobson Station Name	Latitude (°)	Longitude (°)
EUREKA	79.89	-85.93	BARROW	71.32	-156.60
RESOLUTE	74.72	-94.98	FAIRBANKS	64.80	-147.89
SODANKYLA	67.37	26.65	VINDELN	64.25	19.77
SONDRESTROM	67.00	-50.98	REYKJAVIK	64.13	-21.90
VINDELN	64.25	19.77	LERWICK	60.15	-1.15
CHURCHILL	58.75	-94.07	BELSK	51.83	20.78
NORKOPING	58.58	16.12	UCCLE	50.80	4.35
TOMSK	56.48	84.97	HRADEC KRALOVE	50.18	15.83
EDMONTON	53.57	-113.52	HOHENPEISSENBERG	47.80	11.02
MANCHESTER	53.45	-2.26	CARIBOU	46.87	-68.02
GOOSE	53.32	-60.38	AROSA	46.77	-100.75
LINDENBERG	52.22	14.12	BISMARCK	46.77	9.67
DEBILT	52.00	5.18	HAUTE PROVENCE	43.92	5.75
VALENTIA	51.93	-10.25	SAPPORO	43.05	141.33
READING	51.42	-0.96	BOULDER	40.02	-105.25
UCCLE	50.80	4.35	SHIANGHER	39.77	117.00
HRADEC KRALOVE	50.18	15.83	ATHENS	38.00	23.70
POPRAD-GANOVCE	49.03	20.32	WALLOPS ISLAND	37.87	-75.52
SATURNA	48.78	-123.13	SEOUL	37.57	126.95
HOHENPEISSENBERG	47.80	11.02	EL ARENOSILLO	37.10	-6.73
BUDAPEST	47.43	19.18	HANFORD	36.32	-119.63
AROSA	46.77	9.67	NASHVILLE	36.25	-86.57
AOSTA	45.71	7.33	TATENO	36.05	140.13
LONGFENSHAN	44.75	127.60	QUETTA	30.18	66.95
TORONTO	43.78	-79.47	CAIRO	30.08	31.28
KISLOVODSK	43.73	42.66	HURGHADA	27.25	33.72
UNIVERSITY OF TORONTO	43.63	-79.43	NAHA	26.20	127.67
LA CORUNA	43.33	-8.50	KUNMING	25.02	102.68
ROME UNIVERSITY	41.90	12.52	ASWAN	23.97	32.45
ZARAGOZA	41.66	-0.94	HAVANA	23.17	-82.33
THESSALONIKI	40.52	22.97	TAMANRASSET	22.80	5.52
MADRID	40.45	-3.55	MAUNA LOA	19.53	-155.58
ANKARA	39.95	32.88	BANGKOK	13.73	100.57
GODDARD	38.99	-76.83	SINGAPORE	1.33	103.88
MURCIA	38.00	-1.17	NAIROBI	-1.27	36.80
EL ARENOSILLO	37.10	-6.73	DARWIN	-12.47	130.83

Atmospheric
Measurement
Techniques

Open Access

EGU

Discussions

MT WALIGUAN	36.17	100.53	SAMOA	-14.25	-170.57
POHANG	36.03	129.38	IRENE	-25.25	28.22
MRSA MTROUH	31.33	27.22	BRISBANE	-27.47	153.03
NEW DELHI	28.63	77.22	SPRINGBOK	-29.67	17.90
SANTA CRUZ	28.35	-16.29	SALTO	-31.58	-57.95
CAPE D'AGUILAR	22.18	114.23	PERTH	-31.95	115.85
PARAMARIBO	5.78	-55.20	BUENOS-AIRES	-34.58	-58.48
PETALING JAYA	3.10	101.65	MELBOURNE	-37.48	144.58
SAN MARTIN	-68.13	-67.10	LAUDER	-45.03	169.68
ZHONGSHAN	-69.40	76.35	COMODORO RIVADAVIA	-45.78	-67.50
AMUNDSEN-SCOTT	-89.98	-24.80	MACQUARIE ISLAND	-54.48	158.97
			USHUAIA	-54.85	-68.31
			VERNADSKY-FARADAY	-65.25	-64.27
			SYOWA	-69.00	39.58
			HALLEY BAY	-75.52	-26.73
			ARRIVAL HEIGHTS	-77.83	166.40
			AMUNDSEN-SCOTT	-89.98	-24.80

Atmospheric
Measurement
Techniques
Discussions

Open Access

Table 3: List of the eight SAOZ stations used for the IASI total ozone column validation.

Stations	Latitude (°)	Longitude (°)	Altitude (m)
Scoresby Sund	70.5	-22.0	67
Sodankyla	67.4	26.6	170
OHP	43.9	5.7	683
Reunion	-20.9	55.5	110
Bauru	-22.3	-49.0	640
Kerguelen	-49.4	70.3	36
Rio Gallegos	-51.6	-69.3	15
Dumont d'Urville	-66.7	140.0	45

Table 4: Mean relative differences and standard deviation in percent between IASI-A and SAOZ total ozone for different latitude zones and day time measurements. The Root-Mean-Square (RMS) in percent is indicated in parenthesis.

Latitude band	Bias (%)
60°N-70°N	6.8 ± 2.8 (7.4)
30°N-60°N	3.8 ± 1.4 (4.0)
0°S-30°S	4.1 ± 1.2 (4.3)
30°S-60°S	1.6 ± 1.0 (1.9)
60°S-70°S	7.6 ± 3.6 (8.4)

5

Atmospheric
Measurement
Techniques
Discussions

Table 5: Overview of the correlation (R) between IASI and sonde O$_3$ for different latitude bands from the surface up to 3 hPa. The absolute bias (ABIAS), relative bias (RBIAS) and the RMS are also provided. The standard deviation of the difference is also indicated.

		60-90°N	30-60°N	0-30°N	0-30°S	30-60°S	60-90°S
Surface-300 hPa	R	0.63	0.58	0.71	0.80	0.47	0.46
	ABIAS (DU)	-2.0±6.0	-4.3±6.0	-3.2±4.1	-3.0±3.7	-2.8±4.3	0.3±4.1
	RBIAS (%)	-5.5±19.1	-13.6±18.1	-13.5±17.0	-13.5±15.7	-11.6±19.1	2.3±20.0
	RMS (%)	19.9	22.7	21.7	20.7	22.3	20.2
300-150 hPa	R	0.76	0.84	0.64	0.68	0.76	0.70
	ABIAS (DU)	8.4±12.5	-1.4±7.4	-1.6±3.8	-1.7±3.2	-0.4±5.2	4.3±6.1
	RBIAS (%)	20.0±28.2	-4.1±20.7	3.4±40.6	-8.2.±36.5	-0.5±24.6	22.0±29.8
	RMS (%)	34.6	21.1	40.7	37.4	24.6	37.0
150-25 hPa	R	0.76	0.88	0.47	0.56	0.83	0.83
	ABIAS (DU)	17.6±39.1	7.1±17.0	5.7±17.2	7.0±12.6	16.2±17.4	39.0±25.4
	RBIAS (%)	10.8±21.2	5.5±11.7	11.0±19.6	11.7±15.1	13.3±14.8	47.0±31.2
	RMS (%)	23.8	12.9	22.5	19.1	19.9	56.4
25-3 hPa	R	0.24	0.57	0.40	0.35	0.77	0.59
	ABIAS (DU)	2.9±19.8	15.4±14.8	35.4±13.3	33.4±11.7	12.6±12.5	2.6±17.6
	RBIAS (%)	5.0±24.3	15.2±14.6	30.1±17.5	26.9±10.5	12.4±12.7	5.6±24.8
	RMS (%)	24.8	21.1	34.8	28.9	17.8	25.5

Figure captions
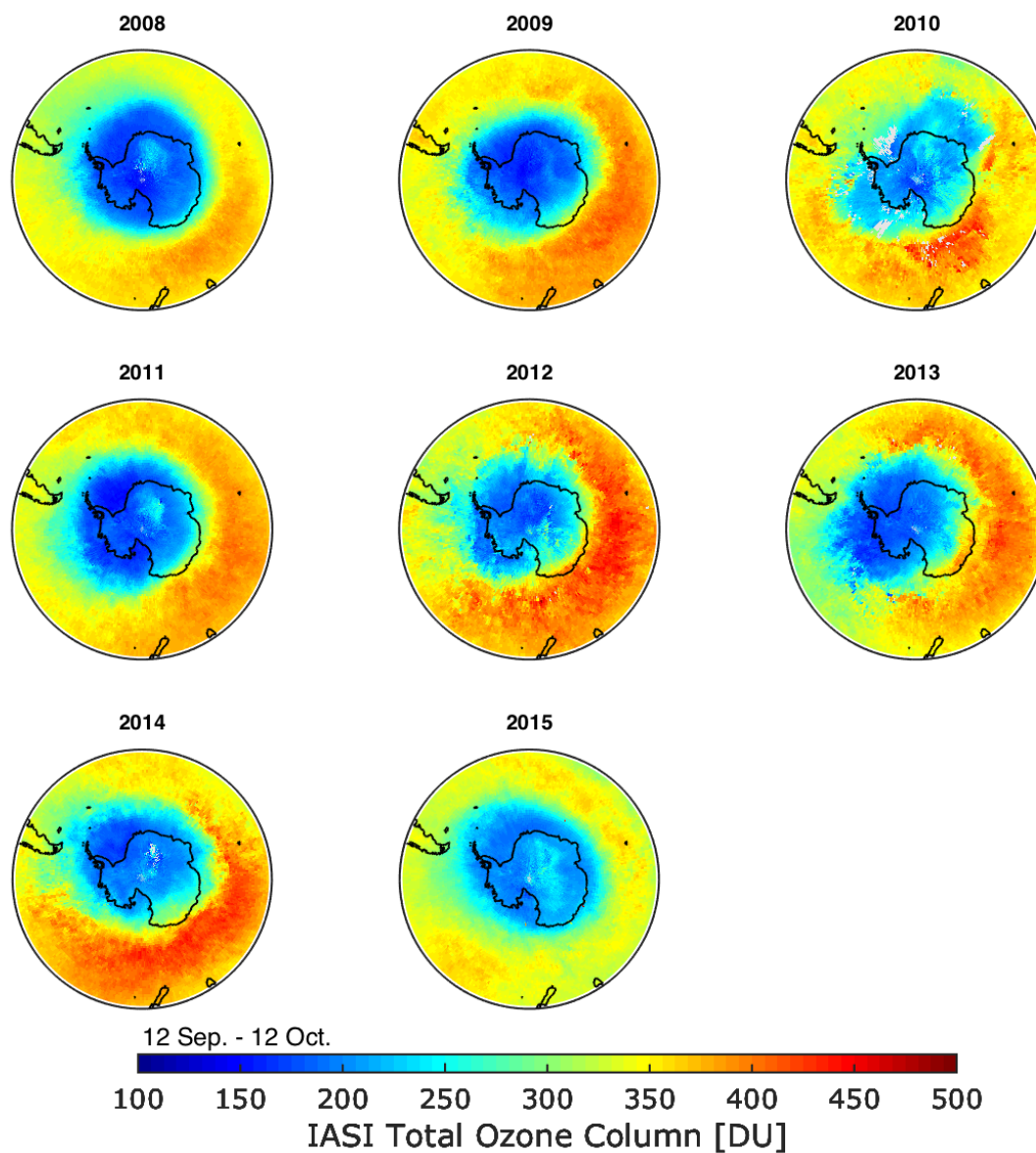
Figure 1: IASI-A averaged total ozone column distribution above Antarctica retrieved using FORLI. Data are averaged over a 1°x1° grid and over one month from 12 September to 12 October during the period 2008-2015.

Atmospheric
Measurement
Techniques
Discussions
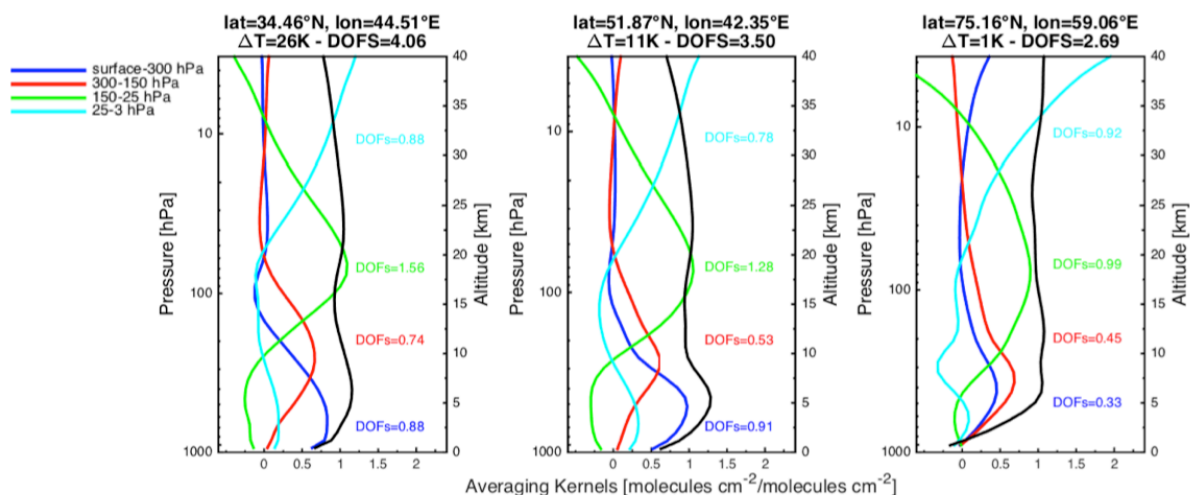
Figure 2: Examples of IASI-A averaging kernel functions associated with high, medium and low thermal contrast for the total ozone column (black) and four different ozone partial columns: surface-300 hPa, 300-150 hPa, 150-25 hPa and 25-3 hPa, characterizing the troposphere (TROPO), the upper troposphere and the lower stratosphere (UTLS), the middle stratosphere (MS) and the upper stratosphere (US), respectively. The averaging kernels correspond to day time measurements obtained on 15 July 2014.
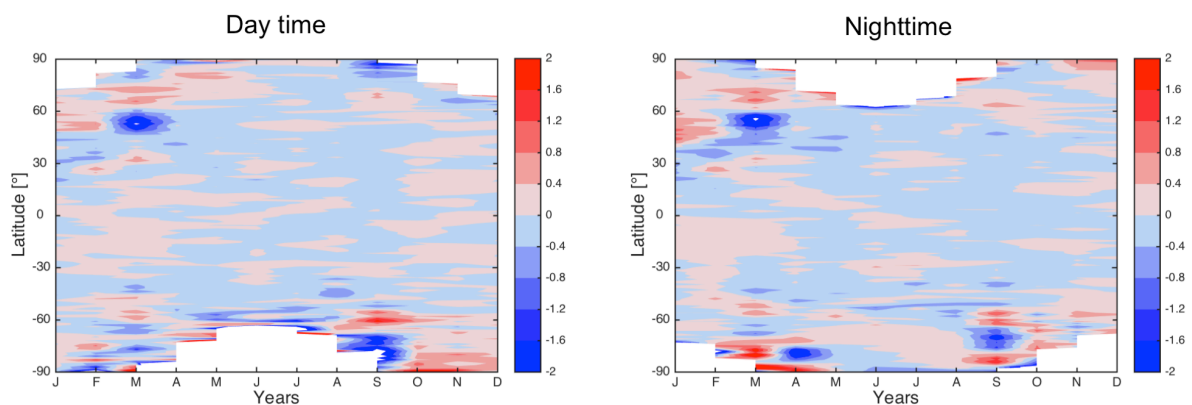
Figure 3: Contour representation of the relative difference (in percent) between IASI-A and IASI-B total ozone column retrieved using FORLI as a function of latitude and time for the year 2014 for day time data (left) and nighttime data (right). The relative differences are calculated as 100 x (IASI-A - IASI-B) / IASI-A.

33

Atmospheric
Measurement
Techniques
Discussions
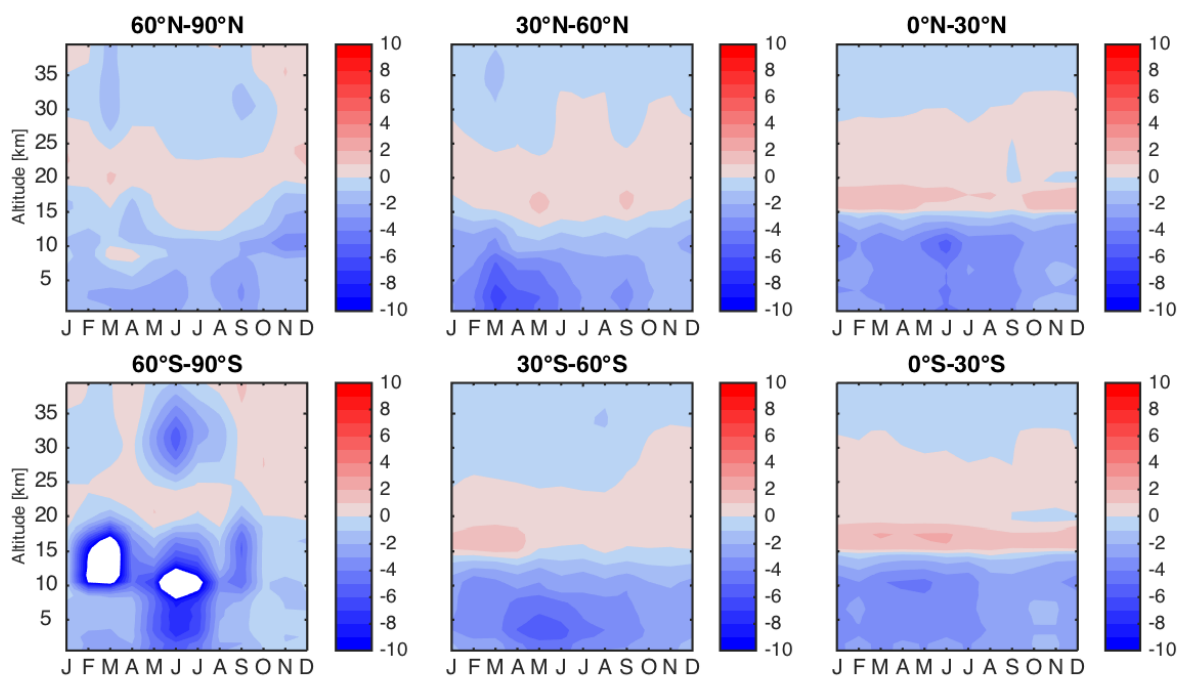
Figure 4: Contour representation of the relative difference (in percent) between IASI-A and IASI-B ozone concentrations as a function of altitude and time for the year 2014 for day time data. The relative differences are calculated as 100 x (IASI-A - IASI-B) / IASI-A. The white area located in the Southern high latitudes corresponds to differences ranging between -20% and -10%.

5

Atmospheric
Measurement
Techniques

Open Access

EGU

Discussions
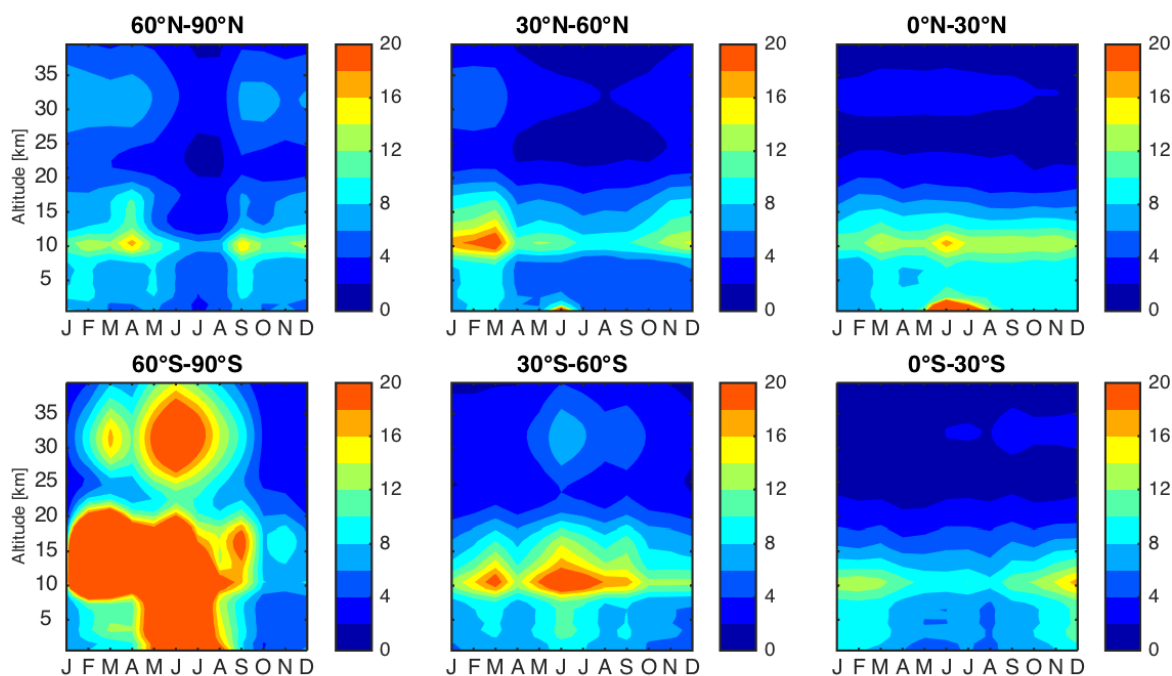
Figure 5: Contour representation of the standard deviation of the differences shown in Fig. 4 (in percent) as a function of altitude and time for the year 2014 for day time data.

Atmospheric
Measurement
Techniques
Discussions
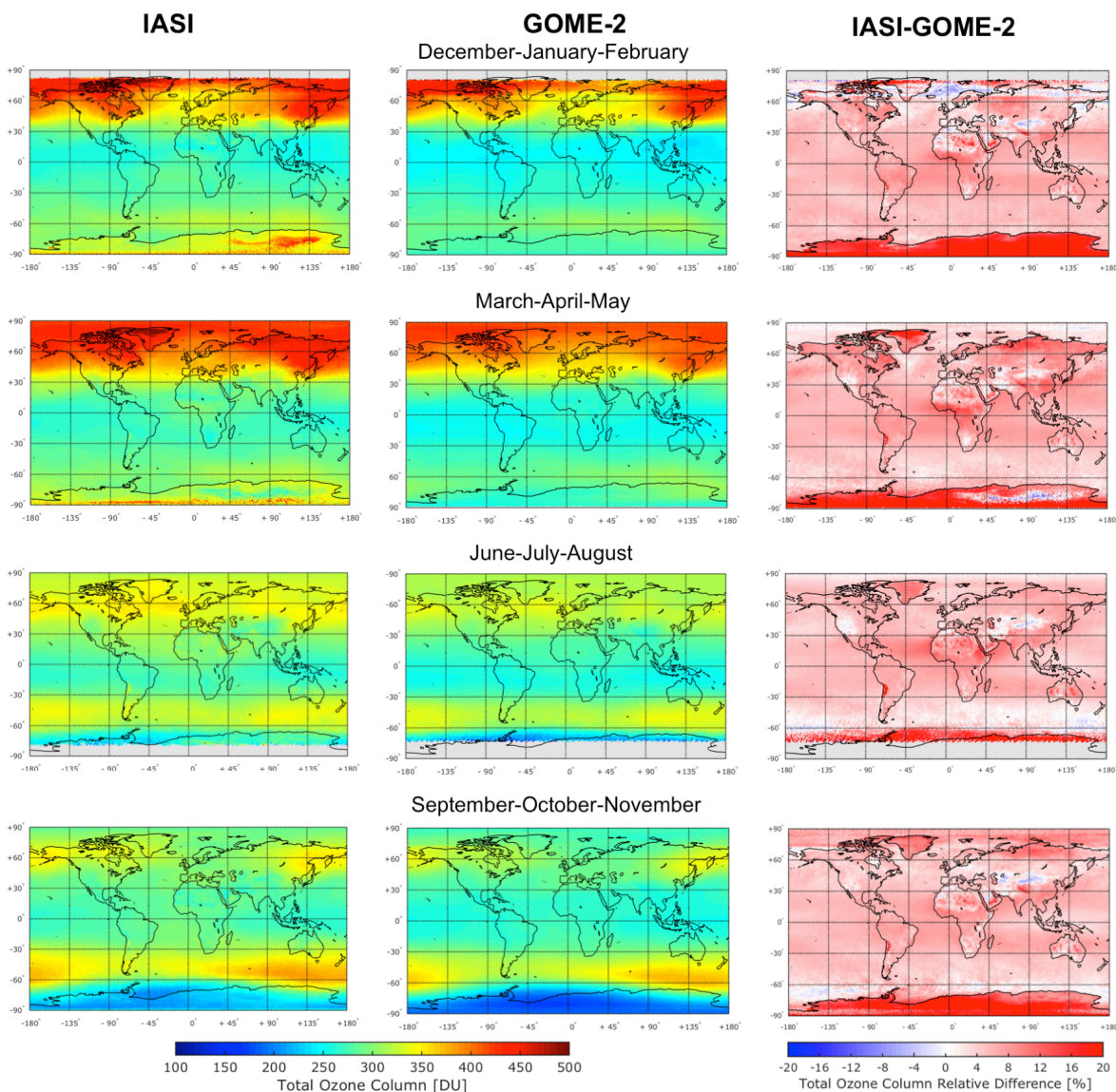
Figure 6: Global distribution for three months averaged periods (1°x1° grid) between 2008 and 2014: (left) IASI-A total ozone column compared to (middle) GOME-2A O3M SAF retrieved total ozone columns for day time observations. The relative differences (in percent) calculated as (IASI-GOME2) / GOME2 x 100 are displayed on the right panels.

Atmospheric
Measurement
Techniques
Discussions
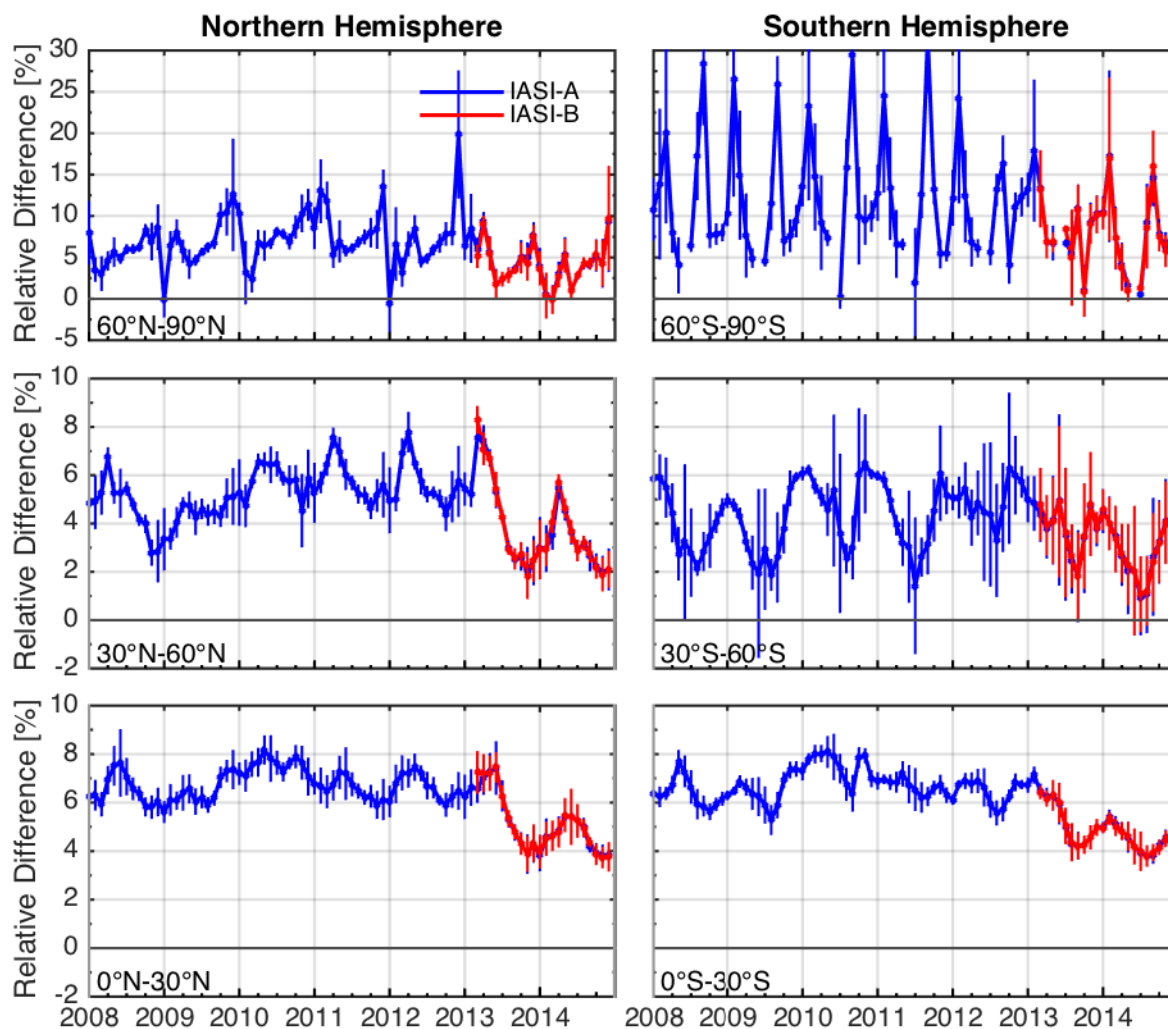
Figure 7: Timeseries of the relative differences between IASI-A (blue) and IASI-B (red) against GOME-2A O3M SAF total ozone columns for different latitudinal bands. The associated standard deviation is also displayed.

Atmospheric
Measurement
Techniques
Discussions
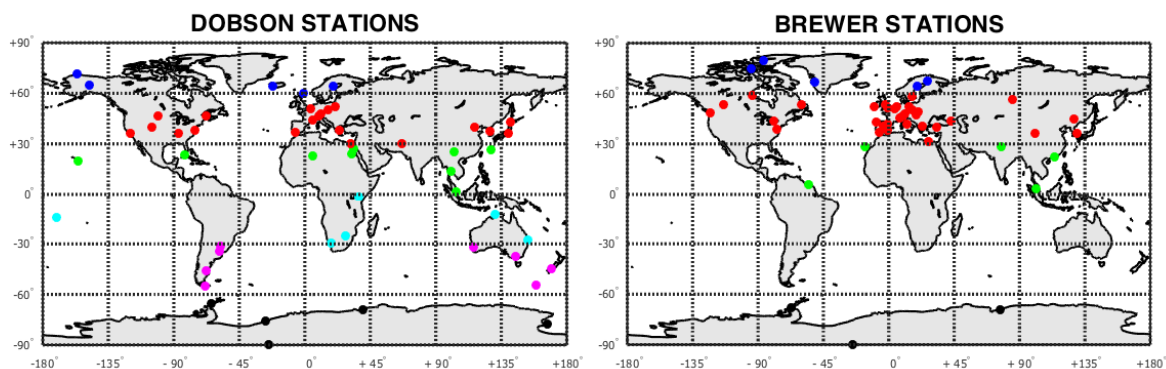
Figure 8: Location of the WOUDC network of ground-based stations used in the present validation exercice; Dobson stations are shown on the left and Brewer stations on the right. The colors indicate different latitude bands: 60-90°N (blue), 30-60°N (red), 0-30°N (green), 0-30°S (cyan), 30-60°S (magenta), 60-90°S (black).

Atmospheric
Measurement
Techniques
Discussions

Open Access
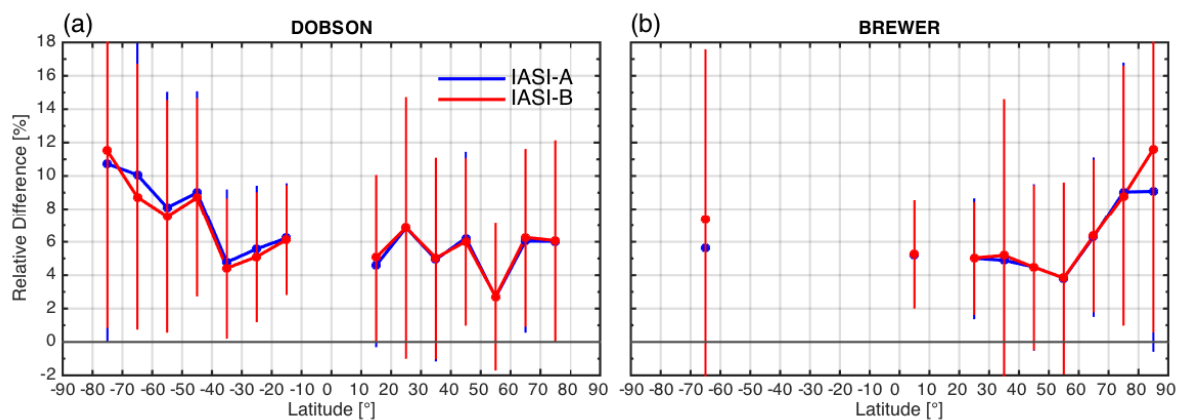
Figure 9: Latitudinal variability of the relative differences (in percent) between IASI-A (blue) and IASI-B (red) against co-located Dobson (a) and Brewer (b) given in bins of 10°. The associated standard deviation of the relative differences is also displayed.

Atmospheric
Measurement
Techniques
Discussions
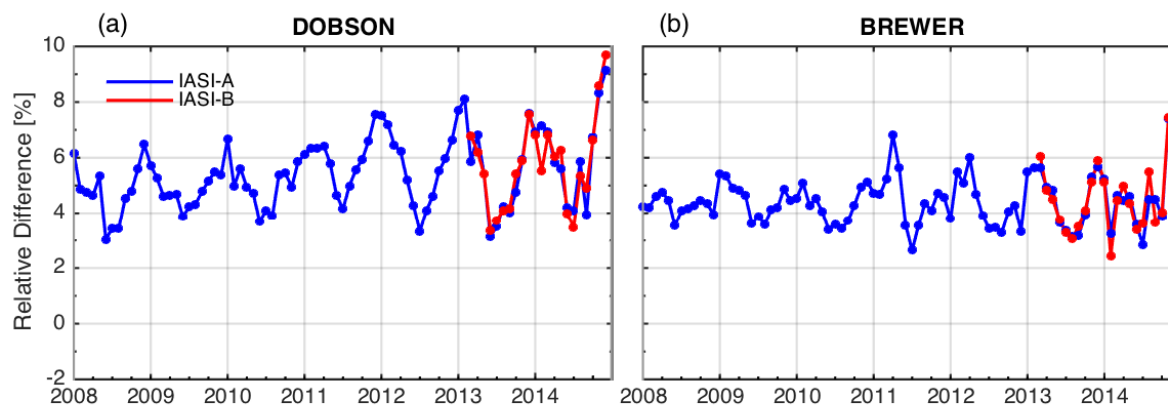
Figure 10: Monthly mean differences (in percent) between IASI-A (blue) and IASI-B (red) TOCs against co-located Dobson (a) and Brewer (b) spectrophotometer TOCs for the Northern hemisphere. For the period March 2013 onwards, only the common co-locations between the two satellites are shown.

5
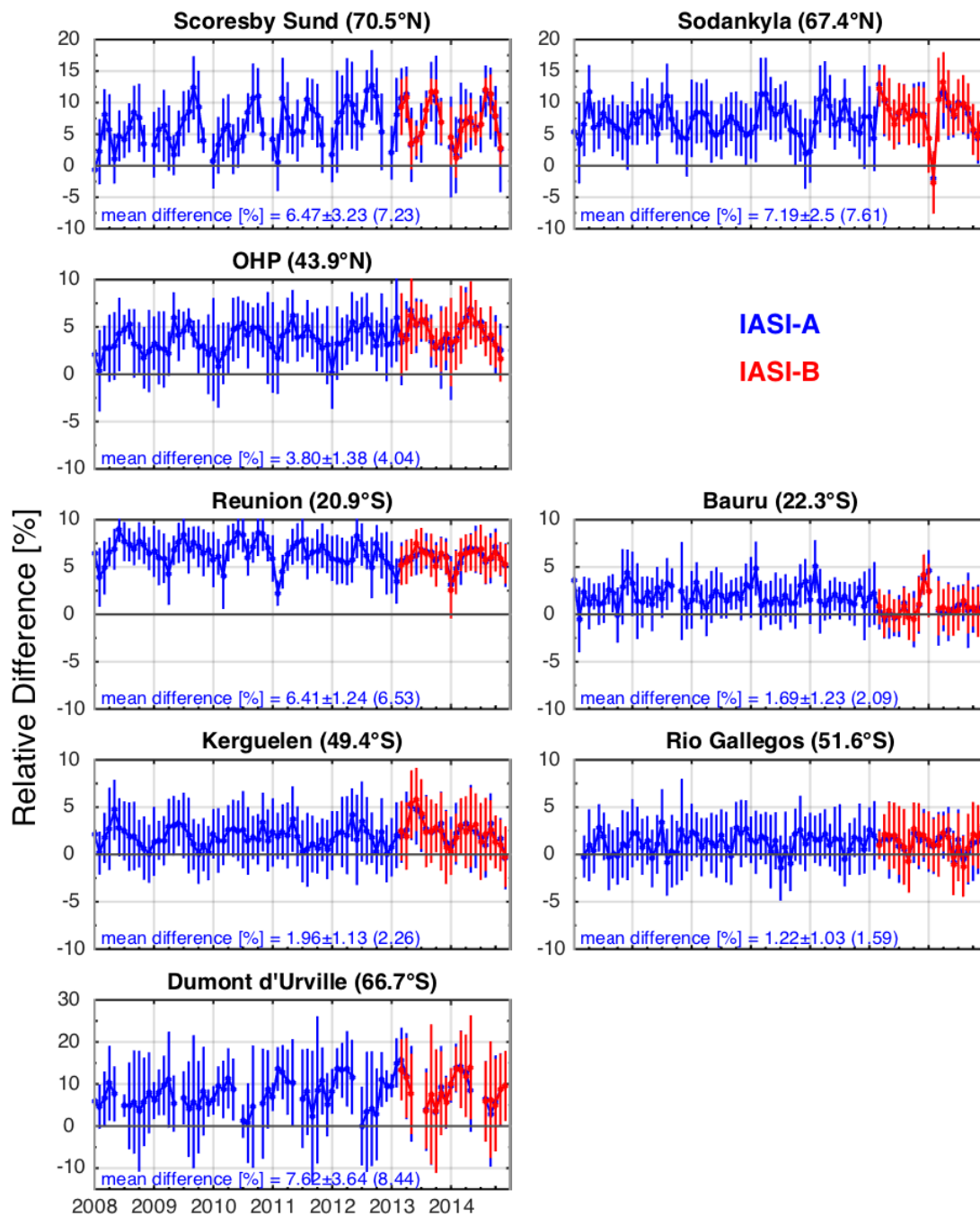
Figure 11: Monthly mean relative differences (in percent) between IASI-A (blue) and IASI-B (red) TOCs against co-located SAOZ TOCs for eight stations from North to South. The associated standard deviation is also displayed. The mean relative difference, standard deviation and Root-Mean-Square (RMS) (in percent) are indicated on each panel. The relative difference (in percent) is calculated as (100 x (IASI – SAOZ) / SAOZ).
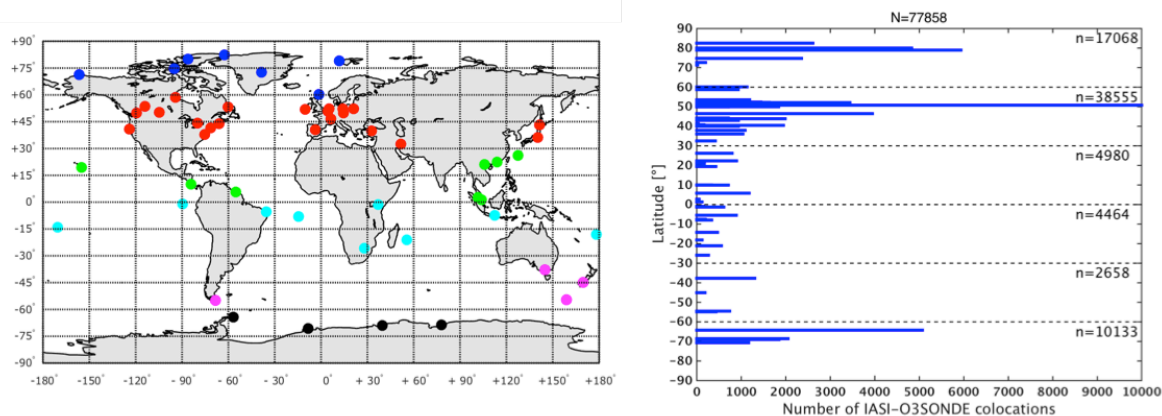
Figure 12: Left: location of the worldwide ozonesonde profiles of WOUDC used in this analysis. The colors indicate different latitude bands: 60-90°N (blue), 30-60°N (red), 0-30°N (green), 0-30°S (cyan), 30-60°S (magenta), 60-90°S (black). Right: distribution of the amount of IASI-A–ozonesonde coincidences available for this study as a function of latitude. The dashed grey lines indicate the latitude boundaries used in this study to evaluate the IASI biases in more detail: the Northern high latitude region: 60-90°N, the Northern middle latitude region : 30-60°N, the Northern tropics 0-30°N and the same symetrically opposite for the Southern hemisphere.

Atmospheric
Measurement
Techniques
Discussions
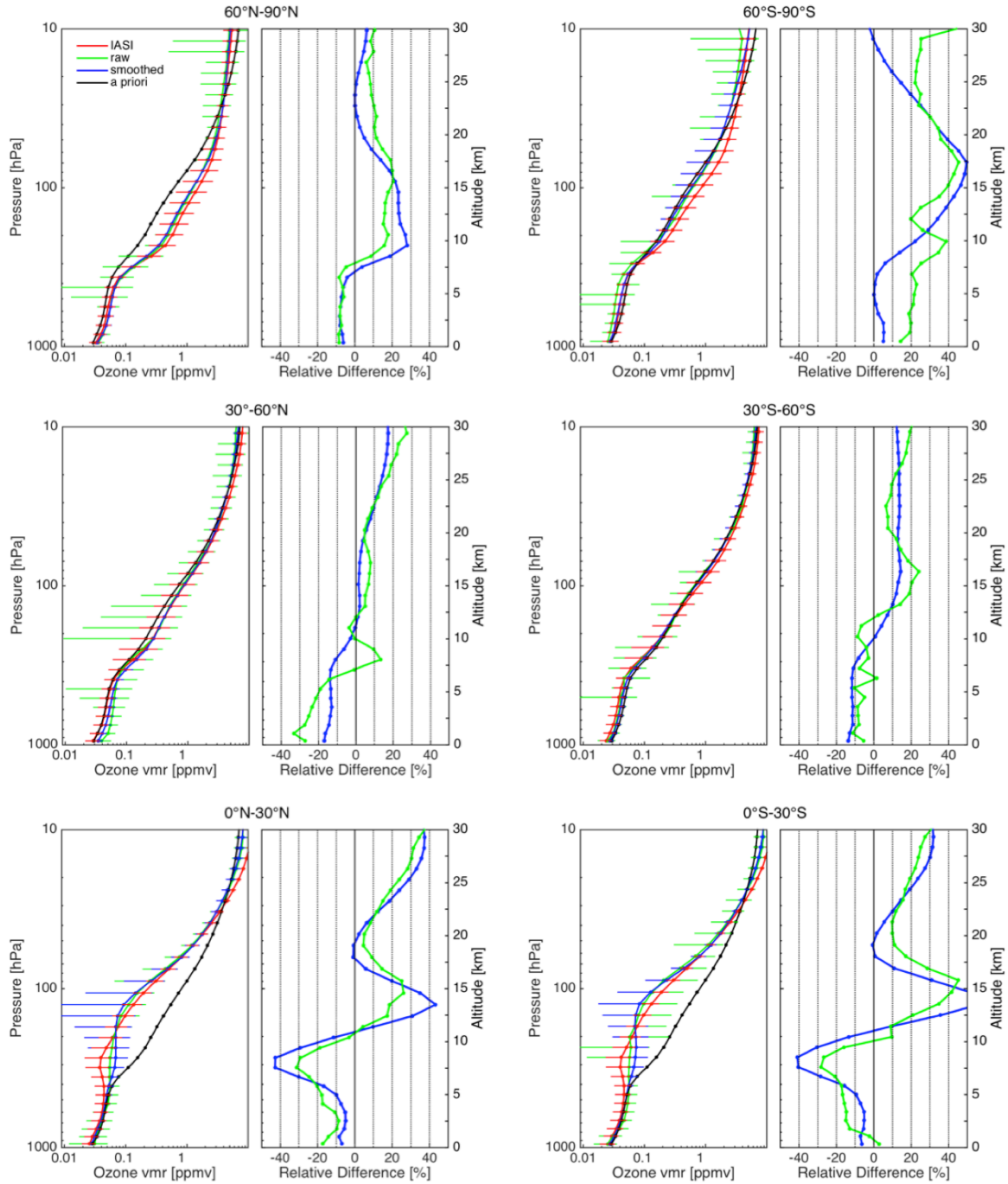
Figure 13: Left panels: Mean ozone vertical profiles retrieved by IASI-A (red), observed by the ozonesondes (green) and observed by the ozonesondes after application of the IASI averaging kernels (blue) for 30° latitude bands. The black line indicates the a priori O$_3$ profiles as used in the IASI retrieval with FORLI. Right panels: Vertical profiles of the relative difference (in percent) between the IASI retrieved mean profile and the smoothed ozonesonde mean profile (blue) or the raw ozonesonde mean profile (green).

Atmospheric
Measurement
Techniques
Discussions

Open Access
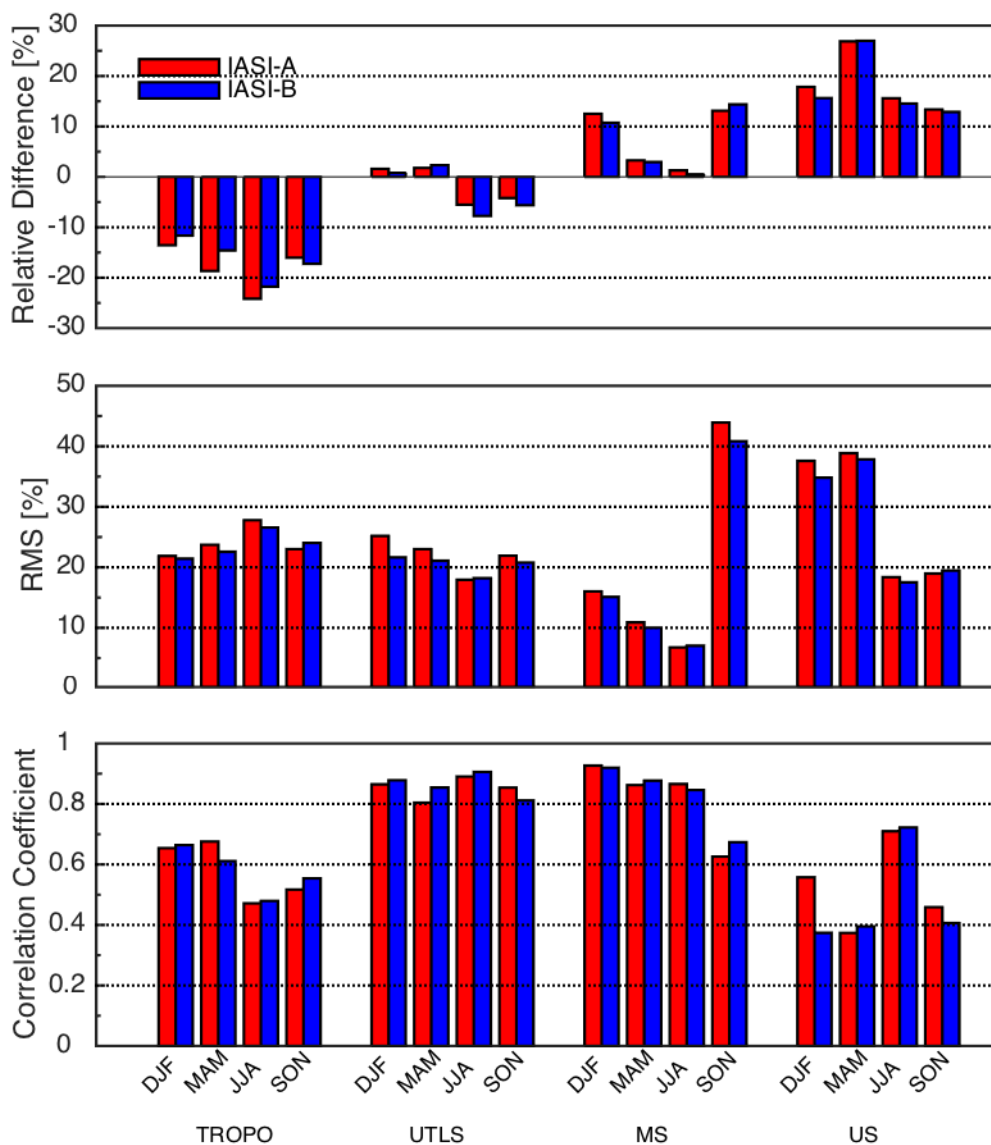
Figure 14: Seasonal variation in the Northern midlatitudes of relative difference (top panel), RMS (middle panel) and correlation coefficient (bottom panel) for the comparison of IASI-A and IASI-B against the smoothed ozonesonde for four different partial columns: surface-300 hPa, 300-150 hPa, 150-25 hPa and 25-3 hPa, characterizing the troposphere (TROPO), the upper troposphere and the lower stratosphere (UTLS), the middle stratosphere (MS) and the upper stratosphere (US), respectively.

5

Atmospheric
Measurement
Techniques
Discussions
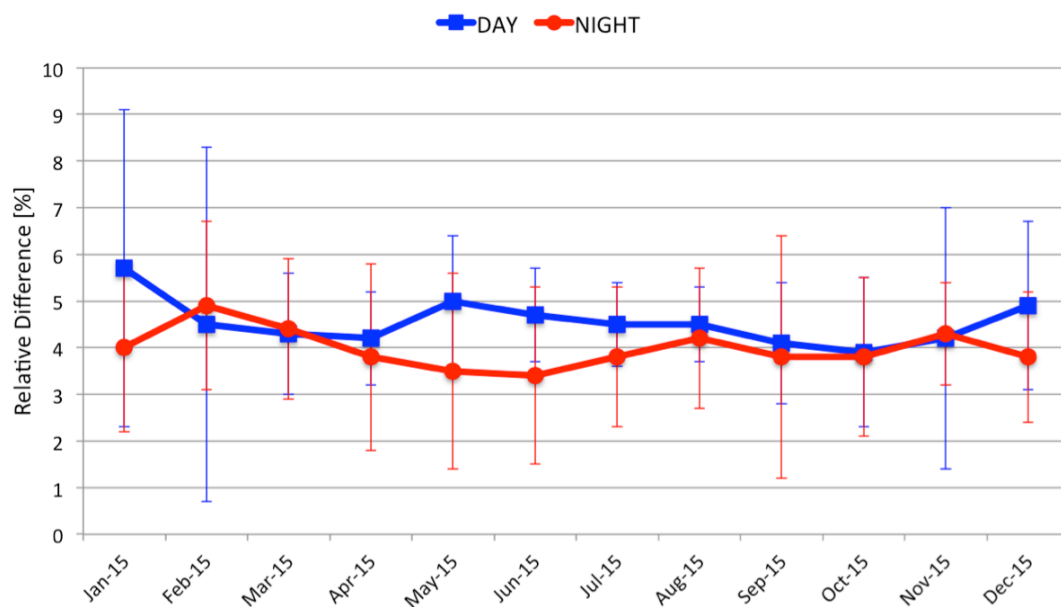
Figure 15: Daily mean relative differences (in percent) between FORLI v20140922 and FORLI v20151001 total ozone columns for day time (blue) and nigthtime (red) IASI measurements for 12 days in 2011 (on the 15th of each month). The relative difference is calculated as :100 x (v20140922 – v20151001) / v20151001.
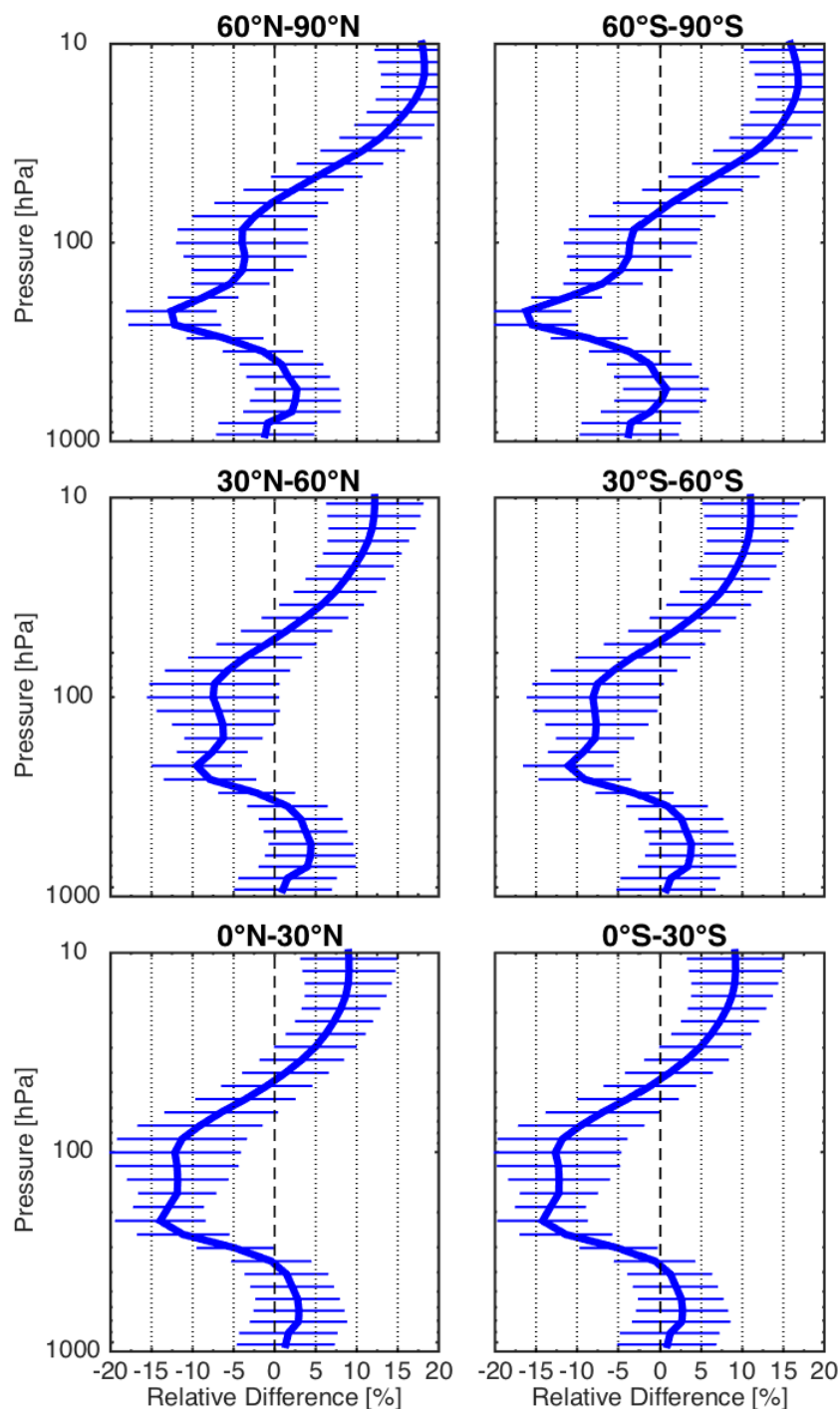
Figure 16: Mean relative differences (in percent) between FORLI v20140922 and FORLI v20151001 averaged over six 30° latitude bands for day time measurements. The standard deviation profiles are overlaid. The relative difference is calculated as : 100 x (v20140922-v20151001) / v20151001.
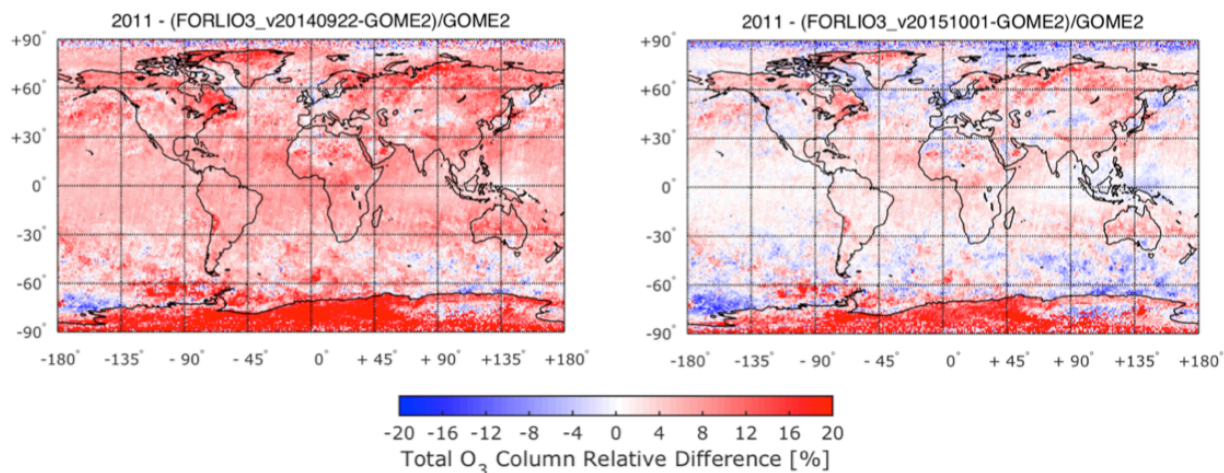
Figure 17: Global distribution of the relative differences (in percent) between FORLI v20140922 (left panel) and FORLI v20151001 (right panel) against GOME-2A O3M SAF TOCs averaged over 12 days of 2011 (on the 15th of each month). The relative difference is calculated as: 100 x (FORLI-O3 – GOME-2) / GOME-2.

47

Atmospheric
Measurement
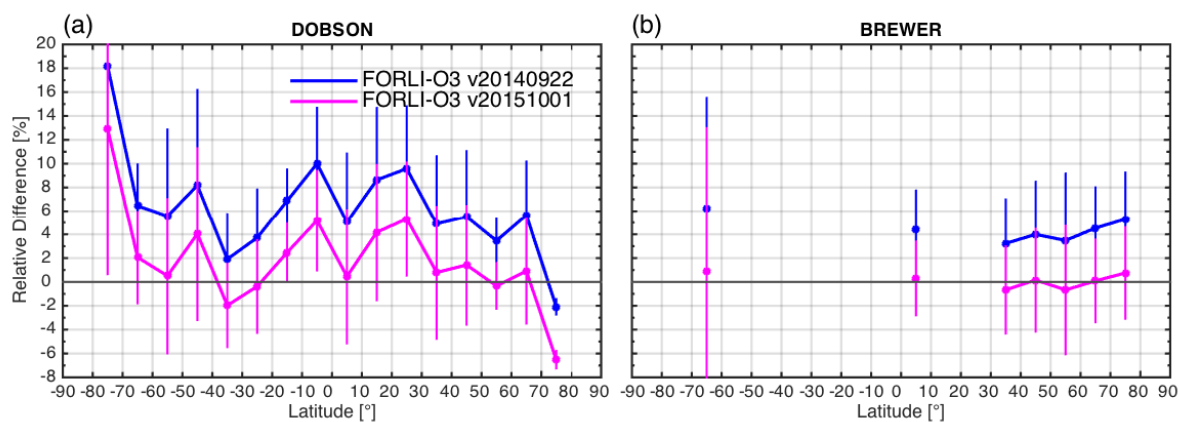Techniques
Discussions
Open Access
EGU

Figure 18: Latitudinal variability of the relative differences (in percent) between FORLI-O3 v20140922 (blue) and FORLI-O3 v20151001 (magenta) against co-located Dobson (a) and Brewer (b) given in bins of 10°. The standard deviation of the relative differences is overlaid. The relative difference is calculated as: 100 x (FORLI-O3 – ground) / ground.
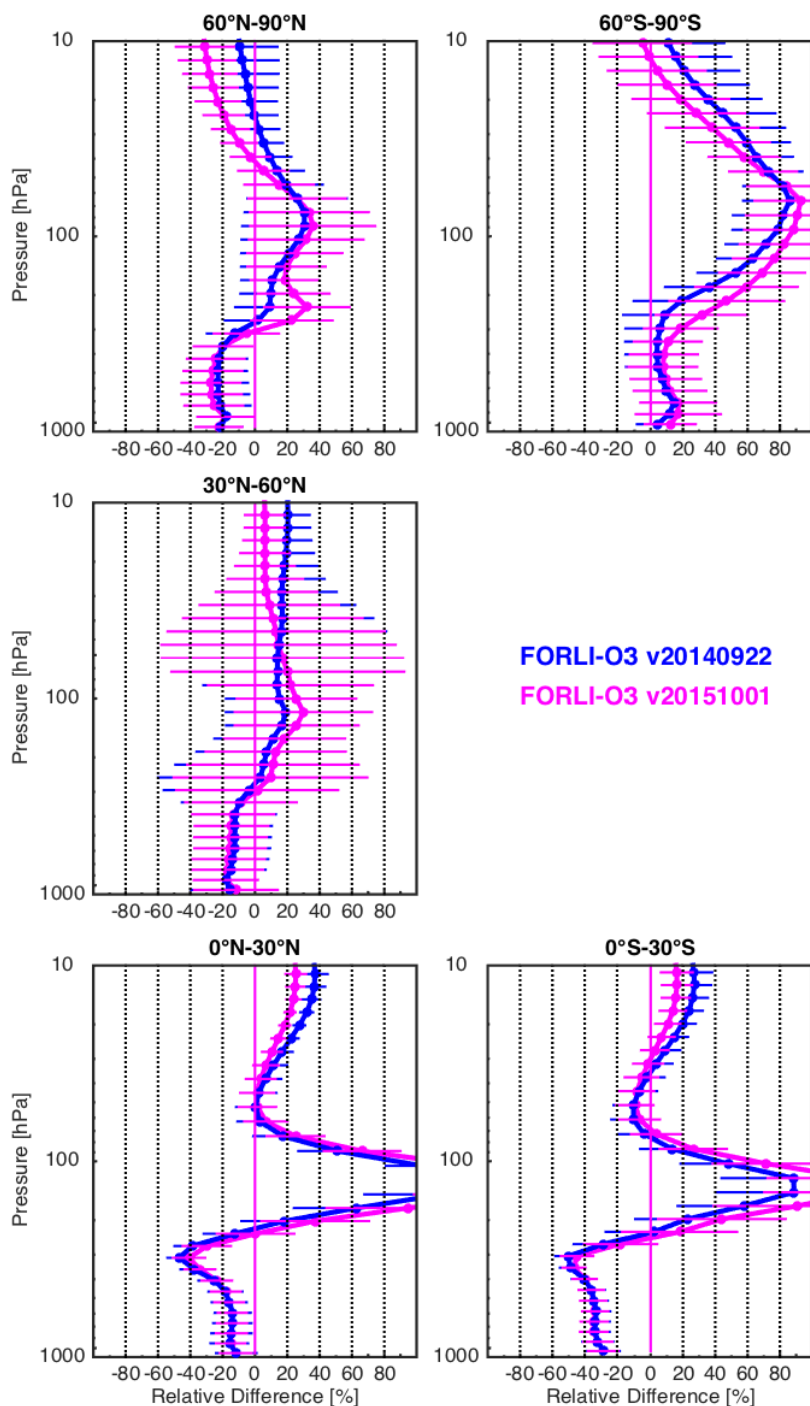
5

Figure 19: Mean relative differences in percent between FORLI-O3 v20140922 (blue) and FORLI-O3 v20151001 (magenta) against sonde ozone vertical profiles for six 30° latitude bands. The standard deviation profiles are also shown. The relative difference is calculated as : 100 x (FORLI-O3 – ozonesonde) / ozonesonde.